Det Kongelige Danske Videnskabernes Selskab
Matematisk-fysiske Meddelelser, bind **30**, nr. 17

Dan. Mat. Fys. Medd. **30**, no. 17 (1956)

MEASUREMENTS OF CONVERSION ELECTRONS FROM COULOMB EXCITATION OF THE ELEMENTS IN THE RARE EARTH REGION

BY

TORBEN HUUS, JØRGEN H. BJERREGAARD,
AND BENT ELBEK

København 1956
i kommission hos Ejnar Munksgaard

CONTENTS

Printed in Denmark.
Bianco Lunos Bogtrykkeri A-S.

The paper deals with the experimental problems connected with measurements of the conversion electrons produced by Coulomb excitation of the heavier elements. It contains the results of a series of measurements on elements with the atomic numbers 25, 26, 47, 60, 62 to 75, and 77 to 79. Reduced transition probabilities are computed from the data and are compared with the results derived from lifetime measurements. By means of the unified model, nuclear moments are calculated from the measured excitation energies and transition probabilities. The values obtained are compared with the theory as well as with other experimental evidence and in general the agreement is found to be satisfactory.

I. Introduction.

The excitation of nuclei by the electric field of impinging heavy particles provides a powerful method for studying the collective nuclear energy spectra. In the two years that have passed since such Coulomb excitation processes were first investigated, one has obtained extensive information* which has yielded many tests of the theoretical predictions based on the unified nuclear model (Bo 1).

According to this model, the collective excitations have a particularly simple character for nuclei possessing large deformations, as encountered in regions far removed from closed shell configurations. Such strongly deformed nuclei are expected to exhibit excitation spectra of simple rotational type, characterized by numerous regularities in energies and transition probabilities. The rotational spectra also have especially small excitation energies and large electric quadrupole matrix elements, making them highly suitable for Coulomb excitation studies.

The region of the periodic table, which offers the best possibility for a systematic study of rotational states by means of Coulomb excitation, is the comparatively large interval between the nuclei having 82 neutrons and mass numbers around $A = 140$, and the doubly closed shell configuration of $_{82}Pb^{208}$. In the present paper, the results of some Coulomb excitation measurements of nuclei in this region are reported.

In the investigation of the radiation from the Coulomb excited

* For a complete list of experimental investigations employing the Coulomb excitation process, the reader is referred to a forthcoming review article (Al 1). We may here especially point to the extensive investigations by N. P. Heydenburg and G. M. Temmer (He 1); C. L. McClelland, H. Mark, and C. Goodman (Mc 1); and P. H. Stelson and F. K. McGowan (St 1).

nuclei we have studied the internal conversion electrons rather than the emitted γ-rays. This method offers the following advantages:

a) The relatively high resolution obtainable with β-spectrometers is useful, in particular when targets of separated isotopes are difficult to obtain, as is the case with the rare earth elements.

b) The presence of lighter elements in the target is comparatively harmless, as a consequence of their small conversion coefficients. This was important in our work since the rare earths were only available in very small quantities and in the form of oxides, which give rise to a γ-ray background under proton bombardment. This background is considerably smaller when α-particles are employed as projectiles which, however, in most instances requires an acceleration voltage of more than the 2 MV at our disposal.

c) The relative intensity of the electrons from the various atomic shells yields information about the multipolarity of the transitions.

On the other hand, the use of the thin targets, which are preferable for the lower electron energies, gives rise to additional uncertainties in the measured cross sections. This is particularly true because of the difficulty of producing stable and homogeneous targets when only very small quantities of the materials are available.

In the present investigation, it was aimed at obtaining a preliminary survey of rotational excitations in the region of the elements considered and, in addition, at estimating nuclear moments on the basis of the observed cross sections. In particular, the trends of the nuclear quadrupole deformations and their relation to the moments of inertia appear to be of interest for current theoretical developments.

In Chapter II, the theory of rotational states and of the Coulomb excitation process is summarized, while the experimental problems are dealt with in Chapter III. The data obtained are tabulated and commented on in Chapter IV, whereas the results are discussed in Chapter V. The theory of a background radiation, important for the measurements, is outlined in the Appendices I and II.

II. Summary of Theory.

A. Rotational States.

In this section, we give a brief summary of the theory of nuclear rotational states, as developed by BOHR and MOTTELSON (Bo 1), and present the formulae which are employed in the present work.

Rotational spectra are associated with nuclei possessing large deformations. For such nuclei one may distinguish between intrinsic and rotational excitations. The former involve a change of configuration of individual particles or vibrations of the nuclear shape, the latter correspond to a collective rotational motion of the nucleus with preservation of the intrinsic structure.

Energy Spectra and Effective Moments of Inertia.

If the nuclear shape possesses axial symmetry, as appears to be the case for all strongly deformed nuclei, the component of the total angular momentum along the symmetry axis is a constant of the motion. The corresponding quantum number 'K' is the same for all the members of a rotational band. For $K \neq 1/2$, the rotational excitation energy ΔE_r is given by

$$\Delta E_r = \frac{\hbar^2}{2\,\Im}\left[I\,(I+1) - K\,(K+1)\right], \tag{1}$$

where I is the total nuclear angular momentum and $\Im$ the effective moment of inertia.

Even-even nuclei have $K = 0$ in their ground state and the corresponding rotational band contains the states

$$I = 0,\ 2,\ 4,\ \ldots \text{ even parity.} \tag{2 a}$$

For odd-A nuclei, or odd-odd nuclei, the spin sequence is

$$I = K,\ K+1,\ K+2,\ \ldots \text{ all same parity,} \tag{2 b}$$

and K thus equals the ground state spin I_0.

In the special case of odd-A nuclei with $K = 1/2$, the spin of the last odd particle is partially decoupled from the rotational

motion. The rotational excitation energy then contains an additional term and is given by

$$\Delta E_a = \Delta E_r + a \cdot \frac{\hbar^2}{2\Im} \cdot \left[1 + (-1)^{I+1/2}(I+1/2)\right], \qquad (3)$$

where the decoupling parameter 'a' is related to the wave function for the last odd nucleon by

$$a = -\sum_j (-1)^{j+1/2}(j+1/2) \cdot |c_j|^2. \qquad (4)$$

In this expression, $|c_j|^2$ represents the probability that the particle possesses a total angular momentum j. The decoupling parameter may be positive or negative, and for $|a| > 1$ formula (3) implies level inversions. Thus, a nucleus with $I_0 = 3/2$ could, in principle, have $K = 1/2$ and an anomalous rotational spectrum.

For rotational spectra of the simple type (1), the ratio of the energies of the second and first excited states depends only on I_0 and is, for odd-A nuclei, given by

$$\frac{\Delta E_2}{\Delta E_1} = \frac{2I_0+3}{I_0+1} = \begin{cases} 2.40 & I_0 = 3/2 \\ 2.29 & I_0 = 5/2 \\ 2.22 & I_0 = 7/2. \end{cases} \qquad (5)$$

The separation between rotational and intrinsic motion depends on the smallness of the rotational frequencies as compared with the frequencies of the intrinsic motion. The finiteness of the rotational frequencies thus gives rise to small deviations from the pure rotational spectra. For the strongly deformed nuclei, these deviations from (1) are expected not to exceed one per cent for the lowest rotational states, except in special cases where the rotational motion may be perturbed by a low-lying intrinsic excitation (cf. Ke 1).

The rotational motion of the nucleus is essentially different from that of a rigid body, and may be pictured as a wave travelling around the nuclear surface. The corresponding moment of inertia is appreciably smaller than for rigid rotation and is related to the magnitude of the nuclear deformation. A simple model,

which has been considered, describes the rotational motion in terms of an irrotational flow. For an ellipsoidal nucleus of constant density, one then obtains

$$\Im_{\text{irrot}} = \frac{2}{5} A_2 M_0 (\Delta R)^2, \tag{6}$$

where ΔR is the difference between the major and the minor semi-axis, while A_2 is the nuclear mass number, and M_0 the nucleonic mass.

In a recent more detailed analysis (Bo 2), it has been found, however, that the nuclear shell structure implies deviations from the model of irrotational flow with moments of inertia larger than (6) in magnitude. Empirical data on the relationship between $\Im$ and ΔR may yield information on the 'purity' of the individual particle motion in the nucleus.

Electric Quadrupole Moments and Transition Probabilities.

The reduced transition probabilities B_{E2} for electric quadrupole excitation* are given by the intrinsic quadrupole moment Q_0 through the expressions

$$B_{E2} = \frac{15}{16\pi} e^2 Q_0^2 \frac{I_0}{(I_0+1)(I_0+2)} \qquad I_0 \to I_0 + 1, \tag{7}$$

$$B_{E2} = \frac{15}{8\pi} e^2 Q_0^2 \frac{1}{(2I_0+3)(I_0+2)} \qquad I_0 \to I_0 + 2. \tag{8}$$

The spectroscopically measured quadrupole moment Q is related to Q_0 by

$$Q = \frac{I_0}{I_0+1} \frac{2I_0-1}{2I_0+3} Q_0. \tag{9}$$

These formulae also hold in the case $I_0 = 1/2$.

By comparison with (2), it is seen that such transitions only reach the first excited rotational state in the even-even nuclei, and the first and second in the odd-A nuclei.

* In the present paper, the letter B always denotes the reduced transition probability corresponding to the excitation, and not to the decay.

For a uniformly charged nucleus of spheroidal shape, one has

$$Q_0 = \frac{4}{5} Z_2 R_0 \cdot \Delta R, \tag{10}$$

where $Z_2 e$ is the charge and R_0 the average radius of the nucleus. By eliminating ΔR by means of (6) and putting $R_0 = A_2^{1/3} r_0$, one obtains*

$$\frac{\hbar^2}{2\,\Im_{\text{irrot}}} \cdot Q_0^2 = \frac{4}{5} \frac{Z_2^2}{A_2^{1/3}} \cdot \frac{\hbar^2 \cdot r_0^2}{M_0} \simeq 5 \frac{Z_2^2}{A_2^{1/3}} \text{ keV} \cdot 10^{-48} \text{ cm}^4, \tag{11}$$

which provides a convenient relation for testing the irrotational estimate for $\Im$.

Magnetic Dipole Moments and Transition Probabilities.

The nuclear magnetic moment and the $M1$ transition probabilities between successive rotational states can be expressed in terms of the two gyromagnetic ratios g_K and g_R, of which the first is associated with the intrinsic angular momentum K and the second with the rotational motion.

The ground state magnetic moment is given by

$$\mu = \frac{I_0^2}{I_0 + 1} \cdot g_K + \frac{I_0}{I_0 + 1} \cdot g_R \qquad \text{n. m.}, \tag{12}$$

holding for $K \neq 1/2$. For $K = 1/2$, the moment contains an additional term, similar to that in (3). (Cf., e. g., Ni 1).

For an $M1$ transition from a state I to a state $I + 1$ in a rotational band with $K = I_0 \neq 1/2$, the reduced transition probability is given by

$$B_{M1} = \frac{3}{4\pi} \cdot \left(\frac{e\hbar}{2 M_0 c} \right)^2 \cdot (g_K - g_R)^2 \cdot \frac{I_0^2 \,(I + 1 - I_0)\,(I + 1 + I_0)}{(I + 1)\,(2\,I + 1)}. \tag{13}$$

Thus, from measurements of μ and B_{M1}, one may determine the quantities g_K and g_R. It is of interest to compare g_R with the value

* Here and in the following, we have employed the value $r_0 = 1.20 \cdot 10^{-13}$ cm.

$$(g_R)_{\text{uniform}} = \frac{Z_2}{A_2}, \tag{14}$$

corresponding to a rotational motion of uniformly charged nuclear matter.

For odd-A nuclei, the radiative decay of rotational excitations can be of the mixed $M1 + E2$ type. The mixing ratio is denoted by δ; its square, which gives the ratio of the number of $E2$ gamma quanta to the number of $M1$ quanta emitted in the decay $I + 1 \to I$, is, for $K \neq 1/2$, given by

$$\delta^2 = \frac{3}{20} \frac{1}{I(I+2)} \cdot \left[\frac{(Q_0 \cdot \Delta E) : (\hbar^2/M_0)}{g_K - g_R} \right]^2. \tag{15}$$

With the usual convention (cf., e. g., Bi 1), $(g_K - g_R)$ should be given the same sign as the ratio $Q_0 : \delta$, but if this sign is not known, one can only determine $|g_K - g_R|$.

If one denotes the transitions from the second to the first rotational state by the subscript 21, and those from the first to the ground state by 1, it follows from (15) that

$$\delta_1^2 : \delta_{21}^2 = \left(\frac{\Delta E_1}{\Delta E_{21}} \right)^2 \frac{(I_0 + 1)(I_0 + 3)}{I_0 (I_0 + 2)} = \left\{ \begin{array}{ll} 1.10 & I_0 = 3/2 \\ 1.04 & I_0 = 5/2 \\ 1.02 & I_0 = 7/2 \end{array} \right\} \tag{16}$$

if one inserts the theoretical energy ratios given by (5).

The mixing ratios can either be determined directly from the $K:L$ ratios or from angular correlation measurements. In addition, they can be obtained from the branching ratio of the cascade to cross-over decay of the second rotational state, if that ratio is known for the $E2$ part of the transition. For rotational states, one has for the quadrupole γ-transition probabilities $T_{E2}\{\gamma\}$ the ratio

$$T_{E2}\{\gamma_2\} : T_{E2}\{\gamma_{21}\} = \frac{1}{2} \left(\frac{\Delta E_2}{\Delta E_{21}} \right)^5 \cdot \frac{(2I_0 + 1)(I_0 + 3)}{I_0^2 (2I_0 + 3)}, \tag{17}$$

where subscript 2 denotes the transition from the second rotational state to the ground state. This formula is valid also for $I_0 = 1/2$.

For a rotational spectrum (1), one finds, by means of (5),

$$T_{E2}\{\gamma_2\}:T_{E2}\{\gamma_{21}\} = \left\{\begin{array}{ll} 9.87 & I_0 = 3/2 \\ 5.86 & I_0 = 5/2 \\ 4.21 & I_0 = 7/2\,. \end{array}\right\} \quad (18)$$

B. Internal Conversion.

In order to determine the transition energies from the energies of the electrons ejected from the K, L or M shells of the target atoms by the process of internal conversion, one will of course have to know the corresponding binding energies. We have used the values compiled in the table published by HILL *et al.* (Hi 1). For the L electrons, most weight has been given to the value for the L_I sub-shell in the case of $M1$ transitions, and to the other two sub-shells for $E2$ transitions. The comparison of the values for the transition energy found from the different conversion lines provides a check on the reliability of the energy determinations and shows also whether the transition has been assigned to the right element.

In order to find the total number of nuclei excited in a given state from yield measurements on a conversion line, one will have to know the corresponding decay fraction $\varepsilon\{n\}$, i. e. the fraction of the excitations which de-excite through that particular mode of decay, represented by the principal quantum number 'n' for the atomic shell. If the conversion coefficients $\alpha\{K\}$, $\alpha\{L\}$, $\alpha\{M\}$, etc. are known, one can calculate ε from

$$\varepsilon\{n\} = \frac{\alpha_{M1}\{n\} + \delta^2\alpha_{E2}\{n\}}{\left(1 + \sum_{\nu}\alpha_{M1}\{\nu\}\right) + \delta^2\left(1 + \sum_{\nu}\alpha_{E2}\{\nu\}\right)} \cdot \beta, \quad (19)$$

where β is the branching fraction, i. e. the fraction of the excitations which decays to the final state in question. For the conversion coefficients, we have used the values represented by the curves in Figs. 1 and 2. They are based mainly on the tables of ROSE *et al.* (Ro 1).* In most instances, the conversion coefficients are so large that the K and L conversion lines together

* We are very grateful to Professor ROSE for sending us his results prior to publication.

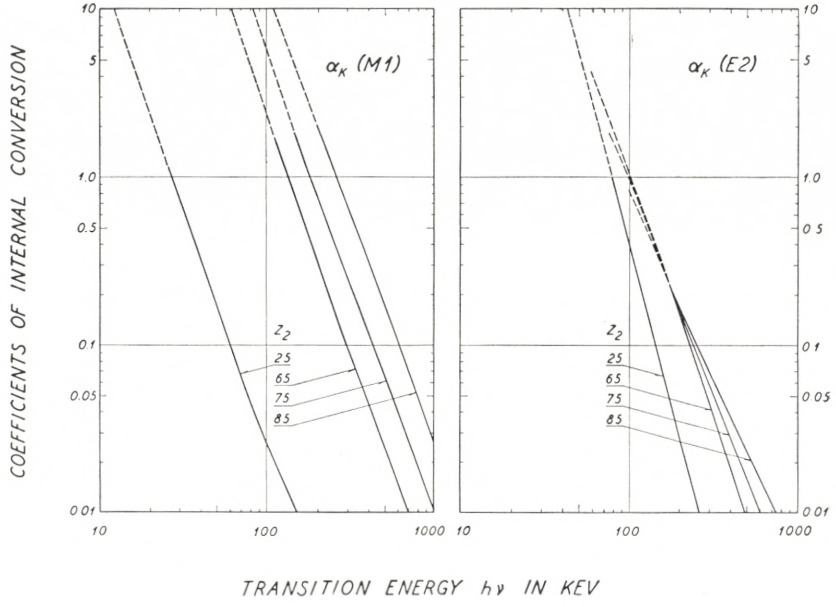

Fig. 1. Internal conversion coefficients for the K shell.* The curves are mainly based on the theoretical results obtained by Rose (Ro 1).

contain the majority of all the decays, which means that $\varepsilon\{K\} + \varepsilon\{L\}$ approaches the value β, almost independent of the conversion coefficients and of δ^2. It is, therefore, important to determine the yield of both these lines or, e. g., the yield of the L line and the $K:L$ ratio.

For the transitions in which a spin change $\Delta I = 2$ is involved, one knows of course that $\delta^2 = \infty$ and, since the $E2$ transitions ordinarily have conversion coefficients corresponding to $K:L < 1$, one can in general obtain a good transition yield determination from the theoretical $K:L$ ratio and measurements on the L line. For the case $\Delta I = 1$, the value of δ^2 is not known a priori, and one will have to measure the $K:L$ ratio also. Thereby one obtains, however, an explicit value of δ^2, since one has

$$\delta^2 = \frac{\alpha_{M1}\{K\}}{\alpha_{E2}\{K\}} \cdot \frac{(L:K)_{\text{obs}} - (L:K)_{M1}}{(L:K)_{E2} - (L:K)_{\text{obs}}}, \tag{20}$$

* Note added in proof. It seems that the finite size of the nucleus gives rise to a significant correction to the $M1$ coefficients which, for $Z_2 \simeq 70$, should be about 25 per cent smaller than given by Fig. 1 (cf. Al 1). The effects on the $K:L$ ratios and the $E2$ coefficients are considerably smaller.

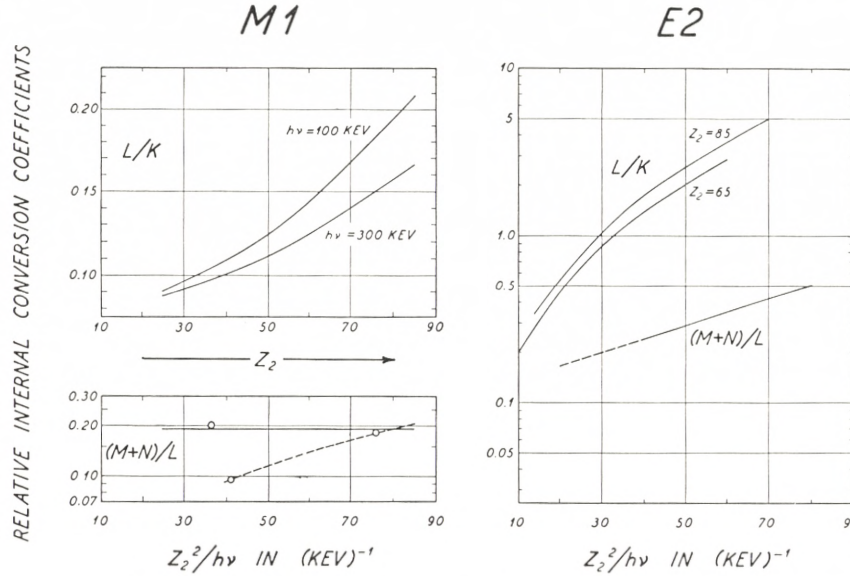

Fig. 2. Semi-empirical ratios for the internal conversion coefficients for the various shells. In the case of the $L:K$ ratios the values are based mainly on the work of Rose (Ro 1)*. For the $M1$ radiation, it should be mentioned that the 500 keV curve is falling in between the 100 keV and 300 keV curves. For the $E2$ radiation, the $Z_2 = 65$ curve is based mainly on empirical data. In the case of the $(M + N):L$ ratios we have taken the values from the paper of H. de Waard (Wa 1), with the exception that, for the $M1$ radiation, we have employed the full drawn curve, which seems as reasonable as the dashed curve given by de Waard.

where $L:K$ stands for the corresponding ratio of the conversion coefficients. In this way, one is able to determine the magnetic matrix element in terms of the quadrupole matrix element. In order to obtain absolute values for these matrix elements from the measured cross sections, the branching fraction β must also be known (cf. (19)). For the first excited state, we have $\beta = 1$, and for the second excited state, the branching can be determined in terms of δ^2 for the mixed transitions, as one has

$$\frac{\beta_{21}}{1-\beta_{21}} = \frac{\beta_{21}}{\beta_2} = \frac{\left(1+\sum_{\nu}\alpha_{M1}\{\nu_{21}\}\right):\delta_{21}^2 + \left(1+\sum_{\nu}\alpha_{E2}\{\nu_{21}\}\right)}{1+\sum_{\nu}\alpha_{E2}\{\nu_2\}} \cdot \frac{T_{E2}\{\gamma_{21}\}}{T_{E2}\{\gamma_2\}}, \quad (21)$$

where $T_{E2}\{\gamma_{21}\}:T_{E2}\{\gamma_2\}$ is given by formula (17) from the theory for the rotational states. If β_{21} is close to unity, the simul-

* Note added in proof. All L shell coefficients have now been computed also for $Z_2 = 55$. For the $E2$ transitions, the $L:K$ ratios come out about 1.5 times smaller than corresponding to the Z_2 dependence indicated in Fig. 2.

taneous measurements on the cascade and the cross-over lines lead to the best determination of $(g_K - g_R)$ through the equation (21), which essentially provides a means of comparing this quantity with the value of Q_0 determined from the excitation of the second excited state. Which way the above formulae are used in the present work depends on the particular example; usually, however, it is most convenient to test the nuclear theory by determining δ^2 from $K:L$ and β from δ^2, and then to check the consistency of the results by comparing the Q_0-values obtained from the excitation of the first and second excited states.

C. Electromagnetic Excitations.

If one bombards nuclei having the charge $Z_2 e$ by projectiles with the charge $Z_1 e$ and an energy E_1 small compared to the Coulomb barrier, i. e.,

$$E_1 < \frac{Z_1 Z_2}{A_2^{1/3}} \cdot \frac{e^2}{r_0}, \tag{22}$$

then the predominant process will be the excitation of the nuclei through the effect of the long range electromagnetic forces. The theory for this process has recently been worked out in great detail by ALDER and WINTHER (Al 2). The total excitation cross sections are given by

$$\sigma_{E\lambda} = \left(\frac{b}{2}\right)^{2-2\lambda} \cdot \frac{B_{E\lambda}}{e^2} \cdot \left(\frac{Z_1 e^2}{\hbar v_i}\right)^2 \cdot \left(\frac{v_f}{v_i}\right)^{2\lambda-2} \cdot f_{E\lambda}\{\xi\} \tag{23}$$

$$\sigma_{M\lambda} = \left(\frac{b}{2}\right)^{2-2\lambda} \cdot \frac{B_{M\lambda}}{e^2} \cdot \left(\frac{Z_1 e^2}{\hbar c}\right)^2 \cdot \left(\frac{v_f}{v_i}\right)^{2\lambda-2} \cdot f_{M\lambda}\{\xi\} \tag{24}$$

$$b = \frac{Z_1 Z_2 e^2}{\frac{1}{2} M v_i^2}; \qquad \xi = \frac{Z_1 Z_2 e^2}{\hbar}\left(\frac{1}{v_f} - \frac{1}{v_i}\right). \tag{25}$$

Here, M means the reduced mass, whereas v_i and v_f are the initial and final relative velocities of the projectiles. The dimensionless functions $f\{\xi\}$ are tabulated in the work of ALDER and WINTHER (Al 2), and the values reproduced here in Fig. 3 for

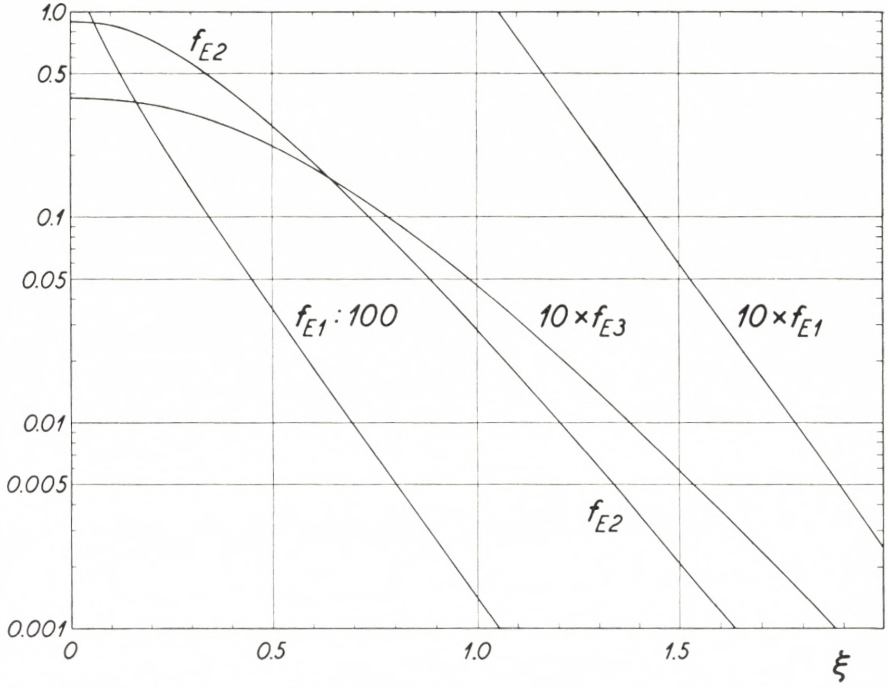

Fig. 3. Curves giving the f-functions defined in the text. The values are taken from the work of ALDER and WINTHER (Al 2).

the electric excitations. The quantities B are the reduced transition probabilities for the excitation.

The collective rotational excitations are of electric quadrupole type. For these, the total cross section can be written in the form

$$\sigma_{E2} = \left(\frac{69.4}{Z_2}\right)^2 \cdot \frac{A_1 (E_1 - \Delta E')}{(1 + A_1 : A_2)^2} \cdot \frac{B_{E2}}{e^2} \cdot f_{E2}\{\xi\} \text{ millibarn}, \quad (26)$$

if one inserts the effective excitation energy $\Delta E'$ and the LAB bombarding energy E_1 in MeV as well as the $B_{E2} : e^2$ in units of 10^{-48} cm^4. The number A_1 here denotes the exact mass of the projectiles in units of the nucleon mass, and $\Delta E'$ is related to the actual excitation energy ΔE by the equation

$$\Delta E' = (1 + A_1 : A_2) \cdot \Delta E. \quad (27)$$

For all types of transitions one has, for the energies in MeV,

$$\xi = \frac{Z_1 A_1^{1/2}}{E_{av}^{3/2}} \cdot \frac{Z_2 \, \Delta E'}{12.65}, \tag{28}$$

where E_{av} is the 'average' bombarding energy defined by

$$E_{av}^{3/2} \equiv \frac{1}{2}\left[\left(1 - \frac{\Delta E'}{E_1}\right)^{1/2} + \left(1 - \frac{\Delta E'}{E_1}\right)\right] \cdot E_1^{3/2} \simeq \left(E_1 - \frac{1}{2}\Delta E'\right)^{3/2}. \tag{29}$$

This means that different projectiles will have very nearly the same ξ-value if only they have bombarding energies in proportion to $Z_1^{2/3} A_1^{1/3}$. Without knowing the value of ΔE, one can therefore determine the multipole order λ of the excitation by comparing the reaction cross sections for bombardments with different particles (Bj 1). With the type of the transition known, one can determine ΔE through the f-function by measuring the excitation function for one kind of particles. Such a procedure may be useful for the interpretation of the results. Combined with measurements where the angular distributions of the emitted radiations have been observed, it allows a rather unambiguous level assignment.

The reduced transition probabilities for the excitations are the same as those for the corresponding de-excitation process, except for a trivial spin weight factor. Their determination from the excitation cross sections is therefore equivalent to measurements of the lifetimes for the decay of the states excited. One has for the transition probability (cf., e. g., Bo 1)

$$T_{E2}\{\gamma\} = 1.23 \cdot 10^{13} \frac{2\,I_0 + 1}{2\,I + 1} \Delta E^5 \frac{B_{E2}}{e^2} \sec^{-1}, \; I \to I_0 \tag{30}$$

if ΔE is inserted in MeV and the $B_{E2}{:}e^2$ for the $E2$ excitation in units of 10^{-48} cm^4. The half-life of the state I is given by

$$\tau_{1/2} = \frac{0.693 \; \varepsilon\{\gamma_{I \to I_0}\}}{(1 + \delta^{-2})\, T_{E2}\{\gamma\}}, \tag{31}$$

where the decay fraction $\varepsilon\{\gamma\}$ for the γ-transition to the ground state of course depends on the mixing ratio δ^2 and the branching fraction β. (Formula (19) can also be used for $\varepsilon\{\gamma\}$ if the α's in the numerator are replaced by unity). It is seen that the con-

version coefficients come in twice when one compares half-lives with excitation cross sections and, for this reason, rather large uncertainties are introduced when these coefficients are only known approximately.

III. Experimental Problems.

A. Calibration of Apparatus.

Two pieces of direct information can immediately be obtained by the detection of a conversion peak in the spectrum of momenta for the electrons emitted from a bombarded target: the energy of the electrons and their rate of production. In the previous chapter, it has been outlined how one can compute the relevant nuclear properties from these data. In the present chapter, we discuss the factors which enter in the determination of the experimental quantities.

The spectrometer which has been used in the present work is shown in Fig. 4. The magnetically analyzed beam of particles accelerated in the 2 MV electrostatic generator (Br 1) enter the spectrometer through the collimator tube C. Each end of this tube is supplied with stops of tungsten foil, both having circular apertures, 2 mm in diameter. They serve to define the position of the beam so that targets placed on the target holder T can be bombarded only on the spot which constitutes the source point for the spectrometer. The collimator tube and the target holder are supported by lucite and given electric potentials of about $+$ 100 volts with respect to the rest of the spectrometer, which is grounded. This is in order to prevent the secondary electrons from seriously distorting the current measurements of the beam integrator. For the same reason, it is necessary to keep the spectrometer chamber under high vacuum by means of a diffusion pump. The target holder can be turned around its axis, allowing up to 12 different targets to be put into the bombarding position.

The fast electrons emitted from the target are analyzed in the magnetic field between the two plane and approximately semicircular pole faces P_1 and P_2, which define a wedge-shaped gap with the axis passing through the source- and focal-points

of the spectrometer. This field has double-focusing properties (Ko 1), viz. in the direction of the field because of the rotational symmetry around the axis, and in the direction of the axis because of the shape of the curves defining the extension of the field where the electrons enter and leave the deflecting region. This type of spectrometer is convenient for the present purpose, because it utilizes a relatively large solid angle and, in addition, permits the source to be 'viewed' easily from the same side as that bombarded.

The number of projectiles scattered from the target and entering through the entrance stop which defines the bunch of electrons accepted by the spectrometer greatly exceeds the number of electrons. A background arises therefore from these heavy particles, if they can reach the counter by one more scattering on the wall of the vacuum chamber. However, in order to trap the majority of them, one only has to place a kind of Venetian blind at the wall opposite to the target and the counter, in the way indicated in the figure. In the few measurements where a crystal and a photomultiplier tube were employed for detection, this system of stops also served to attenuate the effects of stray light. Actually, the bombarded targets often emitted fluorescent light which, e. g., in the case of the various rare earth oxides, was of a very high luminousity and brightly coloured.

In the present investigation, practically all the measurements were made with a Geiger counter as the detector. It had a round window, 7 mm in diameter and covered by a 1 mg/cm^2 mica foil; the limiting stops employed in front of the window were always smaller and had rectangular apertures. The counter cylinder inside the Geiger counter was insulated from the window frame and given a potential of + 100 volts with respect to it. Thereby, the sensitive region of the counter was narrowed, so that a decrease by a factor of three in the efficiency for γ-rays was obtained without changing the efficiency for the electrons which enter through the window.

The current in the magnetizing coils of the spectrometer was used as a measure of the momentum of the electrons focussed on the counter stop. Provided that the current was changed so that it was never decreased and always brought up to the same maximum value before being switched off, the reproducibility

was in general better than $\pm$ 0.5 per cent. The linearity of the scale was checked by measuring the 24.5, 148, and 222 keV conversion lines of the $Th\,(B + C + C'')$ spectrum. The remanence was found to be about 2 per cent of the field corresponding to the 148 keV line. The absolute calibration of the scale was made by frequent measurements on the Coulomb excitation of the 100 keV level in W^{182}. This calibration disagreed about 1 per cent with the ThB measurement. The energy scale used is, however, believed to be correct within about $\pm$ 1 per cent.

The area $P\{n\}$ of a conversion peak 'n' in a spectrum is a measure of the corresponding yield. If the peaks are sharp, one can disregard the back-scattered electrons which will have lost sufficient energy to disappear in the continuous background. The production yield $Y\{n\}$ will thus be given by

$$Y\{n\} = C\{p\} \cdot \frac{P\{n\}}{p} \cdot \frac{z_f \cdot \bar{f}}{\Delta z} \cdot \frac{4\pi}{d\Omega} \cdot \frac{e}{q}, \qquad (32)$$

where the momentum of the conversion electrons is denoted by 'p'. The factor $C\{p\}$ is applied in order to correct for the loss due to the finite probability that the electrons of momentum p cannot penetrate the counter foil. The correction factor used for the 1 mg/cm^2 mica foil is shown in Fig. 5. For the higher momenta, the values are those given by Saxon (Sa 1), whereas the low momentum values have been estimated from measurements on the background electrons (cf. following paragraph). The average dispersion factor $\bar{f}$ was determined from measurements performed with various dimensions of the counter stop; it was found that $\bar{f} \simeq 2.9$ for the electron orbits accepted by the entrance stop shown in Fig. 4. The distance between source and focus was $2\,z_f = 120$ mm and the counter stop generally used had a length of $\Delta z = 3.0$ mm. The effective solid angle $d\Omega$ corresponding to the entrance stop employed was determined by a comparison between the intensity obtained with this stop and that obtained with another stop, which subtended a known solid angle and was so small that no electrons passing through it could get lost in the pole faces or elsewhere. The value found in this way was $d\Omega/4\,\pi = 0.90$ per cent, if one includes also the effect of the

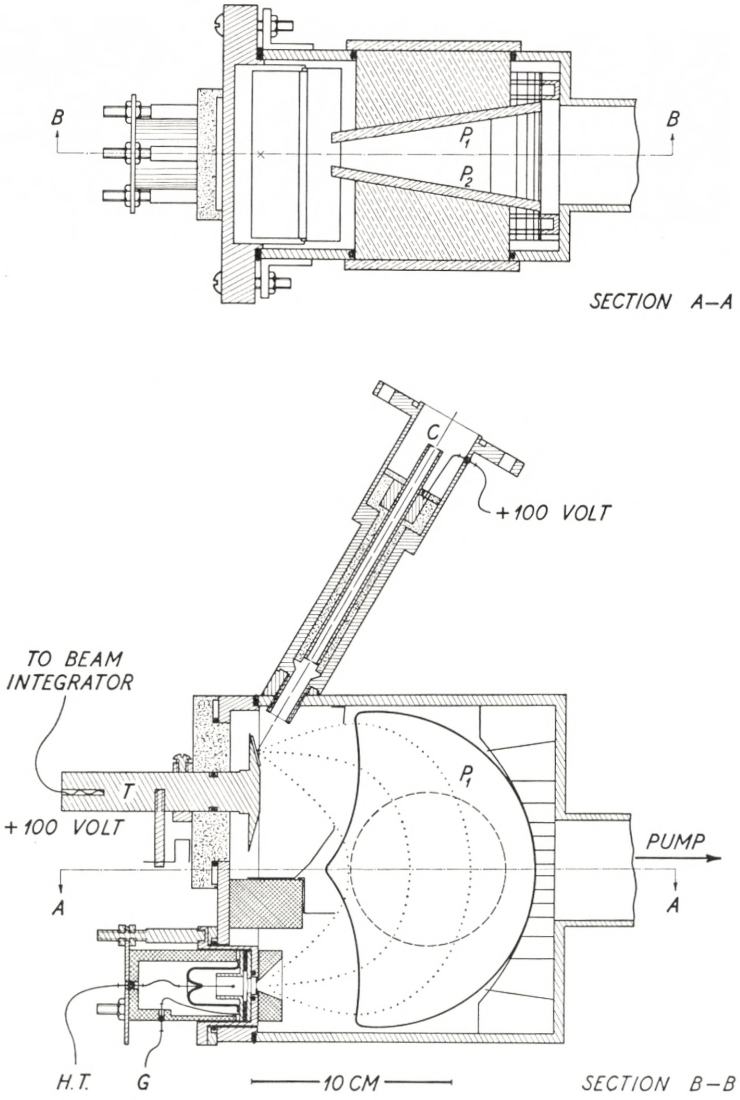

Fig. 4. Beta spectrometer of the wedge-gap type. For a description, confer the text.

finite width of the counter stop, which was $\Delta x = 3.5$ mm. The theoretical angular distributions of the emitted electrons have so far only been evaluated for the K shell (cf. Ro 2, Al 2), and the relatively small effects expected because of anisotropies have therefore been neglected everywhere in the present paper. The last factor in equation (32) contains the total charge 'q' carried

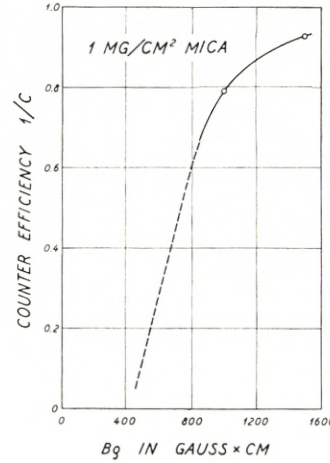

Fig. 5. Counter efficiency of Geiger counter with a 1 mg/cm² mica window. The part of the curve which has been drawn in full is based on the curves given by Saxon (Sa 1). For the extrapolation, confer the text.

by the collected projectiles, and this quantity was measured with a glim-discharge beam integrator, which had proved reliable to within a few per cent.

The Coulomb excitation cross section σ is related to the thin target yield by the equation

$$\sigma \cdot \varepsilon\{n\} = \frac{1}{N} \cdot \frac{d\left(Y\{n\}\right)}{ds}, \tag{33}$$

where $\varepsilon\{n\}$ is the decay fraction (cf. eq. (19)) and N the number of atoms of the kind investigated, which is contained in one cubic centimeter of the target material. The target thickness 's' means the thickness in centimeters measured along the direction of the beam.

In the case of thin targets, it is often more convenient to measure the thickness in mass per unit area. If we denote the thickness, measured in these units and perpendicular to the surface, by 't', then

$$t = s \cdot \varrho \cdot \cos\,\theta, \tag{34}$$

where θ is the angle between the beam and the direction perpendicular to the surface. The specific density ϱ of the target material need not be known when it is the thickness 't' which has been

measured, because in that case only ϱ/N enters in the cross section determination (33). This ratio corresponds to the molecular weight, and is therefore only influenced by the admixture of other atoms in the target, present either in the form of chemical compounds or otherwise.

Direct measurements of 't' by weighing of the targets give only the thicknesses averaged over relative large areas and are, consequently, insensitive to the effects of target inhomogeneities which may have arisen either during the preparation or during the bombardment. As discussed in the last paragraph of this chapter, we have therefore also tried to measure the thicknesses by other means. One method which immediately suggests itself is to employ the background radiation produced in the target atoms (cf. following paragraph).

B. Background Radiation.

In principle, one can reduce as much as wanted background radiations such as that of the scattered projectiles or, e. g., that generated by neutrons in the case of deuteron bombardments. This is not true for the background of electrons produced by the bombardment through direct atomic processes in the target atoms, although the promptness of the ejection of these electrons still provides a means of distinguishing them from the electrons emitted during the more delayed nuclear de-excitation processes (Hu 2). It is therefore important to know in which way the production of these fast stopping electrons is dependent on the experimental conditions.

In the Appendix I, it is shown how one can estimate the probability for the direct ejection of an electron into the continuum with the kinetic energy E_δ by means of a non-relativistic theory neglecting screening effects. To a first approximation, one obtains the following expression for the differential cross section $d\sigma$:

$$\frac{d\sigma}{dE_\delta} \simeq 10^{-18} \cdot Z_1^2 \cdot \left(\frac{E_1}{A_1}\right)^4 \cdot Z_2^4 \cdot \frac{(e^2 \cdot mc^2)^2}{E_\delta^9}, \qquad (35)$$

where the rest energy mc^2 of the electron is introduced for convenience. If one applies the counter foil correction factor (cf.

ref. Sa 1 in the preceding paragraph) to the semi-empirical expression given earlier (Zu 1), one obtains practically the same cross section as that given by the above formula (35). The extrapolated values of the correction factor $C\{p\}$ (cf. Fig. 5) have been obtained from measurements on the stopping electrons, assuming the energy dependence (35) to be valid also at lower electron energies. However, a preliminary measurement, which we have made recently with the Geiger counter replaced by an anthracene scintillation counter, seems to indicate that this procedure leads to reasonable results.

According to formula (35), deuterons should give yields which, under the same conditions, are 16 times smaller than for bombardments with protons. Actually, the yield is found to decrease only by a factor of about 10, but this may not be surprising in view of the experimental uncertainties and the approximations involved in the derivation of the formula (cf. Appendix I). It is nevertheless illustrative for the present purpose to discuss the optimum experimental conditions on the basis of formulae (23), (28), and (35). They imply that the background of stopping electrons depends on the parameters of the bombardment through

$$Z_1^2 \cdot \left(\frac{E_1}{A_1}\right)^4 \simeq \text{const.} \frac{Z_1^{14/3}}{(A_1 \cdot \xi)^{8/3}}. \tag{36}$$

In the case of low-energy conversion lines, where this background will usually be dominant, it obviously is not favourable to go to much higher bombarding energies than those for which the cross sections for Coulomb excitation increase approximately as E_1^4, because then the signal to noise ratio will begin to decrease. For $E2$ excitations, this optimum condition corresponds to $\xi \simeq 0.5$, as is evident from Fig. 6. The equation (36) is a consequence of formula (28) for ξ, which, as mentioned earlier, implies that, in order to obtain a certain ξ-value for a given transition, one will have to employ bombarding energies in proportion to $Z_1^{2/3} A_1^{1/3}$. The maximum signal to noise ratio will thus, for the $E2$ excitations given by (26), be proportional to $(A_1 : Z_1)^4$, which means that deuterons and α-particles should be 16 times better than protons, as far as the influence of the background of stopping electrons is concerned. As mentioned

above, the deuterons are not quite as good as that, and in addition they give the strong 'outer' background due to the neutrons produced (cf. Fig. 10). α-particles will therefore in general be preferable to protons and deuterons in measurements at low electron energies; in addition, at the optimum conditions they have the largest absolute values for the cross sections (cf. Eq. (26)). However, in the search for K-conversion lines, where the corresponding excitation energy is considerably higher than the

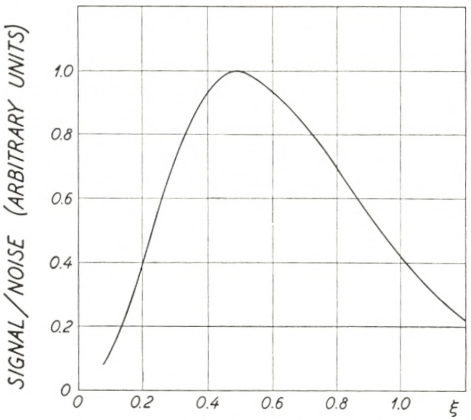

Fig. 6. Relative cross sections for $E2$ Coulomb excitation and the production of stopping electrons, as a function of the bombarding conditions.

electron energy, it often takes a comparatively high bombarding energy to obtain $\xi = 0.5$. The necessary energies are, as shown above, 2.5 times larger for α-particles than for protons, whereas they are only 1.25 times larger for deuterons than for protons. When only a limited acceleration voltage is available it may therefore often occur that the relative smallness of the cross sections then obtainable with α-particles (cf. Eq. (26) or ref. Bj 1) excludes the employment of these projectiles and makes the deuterons best fitted for the purpose.

For the higher electron energies, it will be preferable to bombard with protons and to employ all the acceleration voltage available, since for these electrons the general machine background will usually be more important than the contributions from the stopping electrons. According to equation (26), α-particles can never give $E2$ cross sections more than four times the cross sections corresponding to protons of the same energy,

and as thick targets are preferable here, this advantage will be more than counteracted by the smaller effective target thickness (cf. following paragraph) and the approximately 8 times larger stopping power, which is to be expected for the α-particles.

In order to calculate the thick target yields corresponding to the cross section (35) one must know to what extent the electrons can penetrate the target material. For very thin targets, the yields will of course be proportional to the target thickness, but, as the thickness is increased, the yield of electrons emerging from the surface with a certain energy will increase relatively less. This is due to the fact that the electrons will be scattered and lose energy on their way out of the target, so that those coming from the deeper lying layers will have to be generated with a higher energy, and therefore, according to formula (35), are produced at a much lower rate.

Since the production rate is approximately proportional to E_δ^{-9}, one would expect the effective layer of a thick target to correspond to an energy loss for the electrons of about 10 per cent. However, the scattering of the electrons is so strong in targets of the heavy elements, that their direction of movement is completely changed before they have travelled even this small distance. The way in which the electrons emerge from such targets is thus to some extent similar to a diffusion process. Consequently, the effective target thickness depends most critically on the scattering cross section.

In Appendix II, it is shown that in the diffusion approximation one obtains a yield Y which, for a target thickness t, is related to the corresponding thick target yield Y_∞ by

$$Y \simeq Y_\infty \left[1 - \exp\left\{-t/t_\infty\right\}\right], \tag{37}$$

where the effective thickness t_∞ of the thick target is given by

$$t_\infty \simeq \left(\frac{E_\delta}{50}\right)^2 \text{mg/cm}^2 \tag{38}$$

if one inserts E_δ in keV.* It follows from these equations and from

* The estimate for t_∞ published earlier (Zu 1) does not include the effects of the scattering and is five times larger than (38). However, the neglect of the grain size effect (cf. next paragraph), and an error in the value employed for the dispersion factor practically completely compensated the effect of this overestimate.

(33) — (35) that the thick target yields should be proportional to Z_2^3 in approximate agreement with the experimental findings. We have also checked the above estimates with respect to absolute magnitude, by bombarding silver and gold targets with protons of so high an energy that the thickness (38) can be considered nearly infinitesimal for the projectiles. These elements were

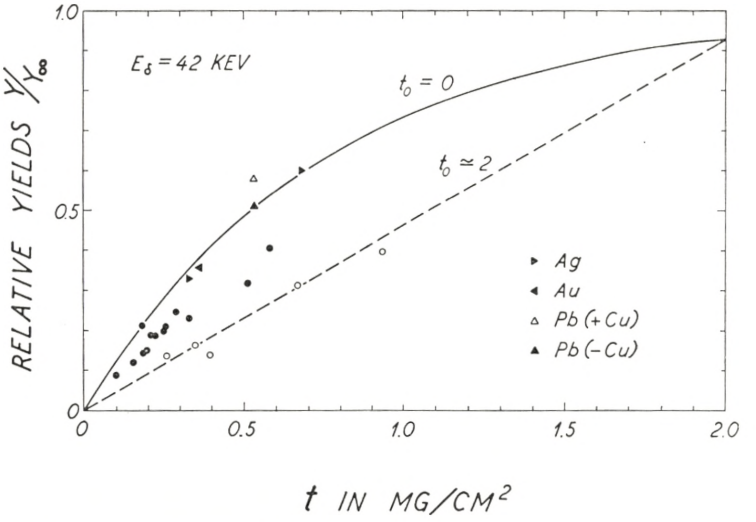

Fig. 7. Thin to thick target yields of stopping electrons emerging from the target surface with an energy of approximately 42 keV. The theoretical variation (37) with the thickness 't' (perpendicular to the surface) of a homogeneous target, is represented by the solid curve. The dashed line indicates the effect of target inhomogeneities corresponding to grain sizes of the order of 2 mg/cm², if 't' is interpreted as the mean thickness. The triangle points correspond to measurements on targets prepared by evaporation; the Ag and Au targets were made on glass, the Pb target on copper. The black circles correspond to measurements on sprayed targets prepared on a support of aluminum; the point on the solid curve corresponds to a target made by means of a particularly thin solution. The open circles correspond to measurements on targets prepared by the suspension method; the yields have been corrected for the contributions from the brass support (cf. the text). For the plotted points, 't' refers to the heavy atoms only.

chosen because they are easy to evaporate onto glass plates in vacuum and give thin targets which are optically homogeneous. The thicknesses were determined by weighing. The result of the comparison is shown in Fig. 7. In view of the approximations involved one would be inclined to consider the good agreement somewhat accidental.

In cases where oxide targets of the type X_2O_3 are used, one

would expect t_∞ to be about 10 per cent smaller than given by (38), so that the thick target yields should be about 80 per cent of the values for the pure targets.

C. Target Preparation and Thickness Determination.

The amounts of the rare earth oxides which were available to us for the target preparation, at the beginning of the present investigation, were in most of the cases only of the order of 10 mg. Attempts to prepare the targets by letting solutions of the materials dry out were not successful; the compounds became deposited as crystals when the evaporation of the liquid was slow, and in very uneven layers when the evaporation was speeded up by heating. Instead, we therefore employed the following more simple technique. We made a suspension of the fine oxide powder in alcohol and allowed proper amounts of it to dry out slowly on small brass disks, which had been pressed down in holes made in a thick rubber plate. Such targets appeared to give relatively reproducible results, but they were certainly not ideally suited for the measurements, especially in view of the effect of the grain size of the oxide powders.

It did not seem likely that reliable thickness determinations could be obtained by means of weighing, since the bombarded area often looked rather damaged when the targets were taken out of the spectrometer after the bombardment. The continuous background of the stopping electrons measured nearly simultaneously with the conversion lines appeared to offer a better measure for the thickness of the targets in the region actually bombarded in the experiment. However, in the beginning we did not realize how important the scattering of the electrons was for the determination of the effective target thickness (38), which we overestimated by a factor of about 5 (cf. Zu 1). Consequently, we ignored the significance of the grain size, and it was only from a closer examination of the continuous background in the measured spectra that it became clear that this was not justified.

The relatively slow variation of $Y : Y_\infty$ as a function of the electron energy, which was found even for small values of this ratio, indicated that the grain sizes were in general comparable

to t_∞ for electron energies as high as 50 keV. A similar behaviour was found for some of the pure metallic targets of, e. g., Ta and W, which had been prepared by evaporation in vacuum and visually showed a clear crystalline structure. For a calibration, it would therefore not be correct to employ the curve in Fig. 7, which corresponds to the homogeneous targets. If one were to idealize the grains as chips of a constant thickness t_0 mg/cm^2 which are not overlapping, then the relative yields would be related linearily to the average thickness $t \leqslant t_0$ in the way indicated by the dashed line in Fig. 7 for the case $t_0 = 2$ mg/cm^2. Investigations of the targets in a microscope showed that the grain sizes were of the general order of 3 microns for the oxides used, corresponding to a diameter of about 2 mg/cm^2, and thus somewhat larger than the estimates derived from (38) and the relative yield dependence.

As long as better targets were not available, we therefore considered it the best compromise to estimate their thicknesses by employing a calibration curve somewhere in between the two curves shown in Fig. 7. In the calculations we first subtracted the full yield of stopping electrons measured for the bare brass support, since this should be correct for the very thin targets, and give errors of only minor importance for the thicker ones. The transition probabilities arrived at in this way could, however, not be expected to be reliable to more than about a factor of 1.5.

Recently, larger samples of most of the rare earth oxides have been put at our disposal by courtesy of Professor Spedding and the Iowa State College.* It has thereby been possible to produce more stable and homogeneous targets, in particular by employing the technique of spraying the dissolved material onto a hot surface.

When preparing the targets by this method we proceeded in the following way. First, a small amount of the oxide powder was dissolved in a few drops of pure concentrated nitric acid which was then heated until only the rare earth nitrate was left. This compound was dissolved in distilled water and put into the bottle of a commercial perfume atomizer, which was adjusted to give the finest possible spray when operated by means of clean compressed

* We are very grateful to Professor Spedding for the great improvement of the measurements, which has been possible in this way.

air. The solution was then sprayed onto the hot surface of a small polished disk of either brass or aluminum, in small bursts of duration of less than a second.

The temperature of the disk is rather critical and should usually be about 300° C. Also the concentration of the solution seemed to be of great importance. With a concentration of about 1 mg per 10 cm^3 of water it was possible to produce rather homogeneous targets on brass supports, but with an efficiency of only about 10 per cent. When such thin solutions were employed with aluminum as the support, we usually did not succeed in making the material condense on the polished surfaces. In these cases, we had to use concentrations of the order of 1 mg per cm^3, which gave rather good efficiencies but, on the other hand, also a somewhat poorer homogeneity. After having finished the spraying we heated the targets to approximately 500° C in order to decompose all the nitrate to the oxide. The targets produced in this way were very stable and usually sufficiently homogeneous within areas of the order of 10 mm^2.

In this manner, we first made a thin target of Yb_2O_3 on a support of brass, which had been covered with a very thin layer of aluminum, so that the target thickness could be determined through a measurement of the energy shift of one of the well-known Al^{27} (p, γ) resonances (the so-called sandwich method). The cross sections for Coulomb excitation, which were found by means of such a thickness calibration, were about three times smaller than the values found previously, and even smaller than those corresponding to the thickness found directly by means of weighing. The latter thickness was, moreover, considerably larger than that determined from the yield of the background electrons by means of the curve in Fig. 7 corresponding to homogeneous targets. These facts indicated that the target did not consist of the pure oxide, but that, in addition, it contained large amounts of light atoms.

It was therefore clear that a method was needed, by which one could determine the number of heavy atoms per unit area independently of the inhomogeneity and composition of the targets. Fortunately, this demand can easily be met through measurements on the spectrum of the elastically scattered projectiles. These particles can penetrate the target layers with energy

losses which are smaller than the energies transferred to the recoils in the collisions with the light atoms. The peak, which in the spectrum of the scattered particles corresponds to the collisions with the heavy atoms, will therefore fall in a region above that in which the contributions from the light atoms are found. Moreover, it will be by far the strongest peak in the spectrum, since the cross section for Rutherford scattering increases as the square of the charge.

We therefore decided to set up a heavy particle spectrometer, which could view the bombarded targets through the pumping tube shown in Fig. 4. The direction of observation formed an angle of 104° with respect to the beam. The spectrometer consists of a 90° deflection magnet with a radius of 42.5 cm. The entrance stop was 2.5 mm in diameter and the distance between this stop and the target 104 cm. The exit slit was placed just outside the end of the plane pole shoes, and was adjusted to a width of 0.85 mm. The particles were detected by means of an anthracene crystal counter. The homogeneous magnetic field was generated by means of permanent magnets, which were magnetized corresponding to an energy of about 1.7 MeV for the protons accepted by the spectrometer. The so-called profile curves were then measured by varying the bombarding energy instead of the spectrometer setting.

An example of a profile curve measured for a thin target of Gd_2O_3 on a support of aluminum is shown in Fig. 8 together with the profile measured for a thick metallic W target. A thick Gd_2O_3 target would have given a yield approximately 50 per cent smaller than that of the thick W target, and the figure therefore shows that the sprayed target gives a maximum yield which is only about half of what it should have been. This clearly demonstrates that the sprayed target is either inhomogeneous, or it contains a large amount of light atoms. A similar result was obtained with the above mentioned Yb_2O_3 target, except for the fact that the profile curve in this case did not go down to zero at the higher bombarding energies. The reason is that in this region the scattering from the brass support gives a contribution which overlaps the peak corresponding to the collisions with the heavy atoms, as a consequence of straggling effects in the target. By means of the profile curve, it was possible to explain

the discrepancies between the previously mentioned thickness determinations for the target as being due to an admixture of larger amounts of light atoms.

It thus appears that thickness calibrations by means of the background electrons are unreliable when the targets are strongly inhomogeneous, whereas the admixture of lighter atoms is of minor importance because they do not contribute very much to

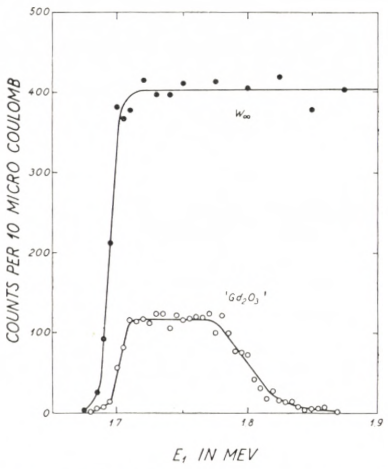

Fig. 8. Profile curves for a thick W target and a sprayed target of Gd_2O_3 (on Al), obtained by measuring the yield of elastically scattered protons as a function of the bombarding energy E_1. The thin target contained 0.26 mg Gd per cm².

either the production or the scattering of the δ-rays. When the thicknesses are determined by the sandwich method or directly by weighing, the situation is the opposite. Here the inhomogeneities are not so dangereous, whereas lack of knowledge about the composition of the target may give rise to larger errors.

The method employing the profile curves should be very reliable, particularly if one uses a light element like aluminum as support. From the measured profiles one can compute the thicknesses in the following way. The peak measured for a pure and homogeneous thin target (such as, e. g., the evaporated Au target mentioned earlier) reaches the thick target yield, and one can determine the thickness directly from the measured half-width when the stopping power of the material is known. As a consequence of inhomogeneities and light element im-

purities the peak will, as we have seen above, be smeared out to a lower and broader one, but in such a way that its area does not change. One can therefore easily determine the half-width which would have been found if the target had been pure and homogeneous; all one has to know is the thick target yield for the pure element. These yields were obtained by extrapolating as $Z_2^{3/2}$ from that found, e. g., for the thick W target, since this dependence is in accordance with both theory and experiment. The accuracy in the thickness determinations by means of this method is therefore only dependent on the energy scale for the accelerated particles, on the relative yields of thin to thick targets, and on the stopping power for the projectiles.

The largest errors are probably introduced through the stopping powers employed. We have used values 10 per cent higher than those obtained from the semi-empirical expression given by C. B. Madsen (Ma 2), since this seems to be in better accordance with the latest experiments. For 1.7 MeV protons on W, the value employed is approximately 50 keV per mg/cm^2. By means of this stopping power we compute for the scattering a theoretical thick target yield which is only about 10 per cent larger than found experimentally. However, the measured yields showed a dependence on the way in which the beam came through the stops of the collimator tube (*C* in Fig. 4), and the absolute yields are therefore not so reliable. For the thickness determination this is of minor importance, since the measured yields were always immediately compared with the thick W yield measured under the same conditions. For the present purpose, the errors in the calibration of the scale of the voltmeter of the electrostatic generator are of no importance.

We repeated the measurements of most of the main conversion lines found in the old thin target experiments with new targets made by spraying the more concentrated of the above mentioned solutions onto 0.5 mm thick disks of aluminum. The yields of background electrons from these targets relative to the corresponding pure thick target yields obtained from interpolations have been compared with the thicknesses determined from the respective profile curves. The result is shown in Fig. 7 and indicates that the new targets were also somewhat inhomogeneous. Comparison between the yield of conversion electrons found in the old and new measurements, respectively, made it possible

to calculate the true average thickness for the old targets, which it was not possible to measure directly because of the fact that they were very inhomogeneous and made on a support of brass. The results obtained for the even elements are shown in Fig. 7. They seem to indicate that the grain diameters in the old targets were of the order of 2 mg/cm^2, in agreement with the microscopic evidence.

For some of the elements, the energies of the conversion electrons are large enough to permit the use of targets which are thick compared to the range of the bombarding particles. In order to determine a nuclear cross section σ from the corresponding thick target yield, it is in general necessary to measure the dependence of this yield on the bombarding energy E_0. However, the absolute value of $\sigma\{E_0\}$ can also be found from a single thick target yield measurement if the relative variation of the cross section is known, so that the theoretical ratio between the thick and thin target yields can be computed. This is the case for the Coulomb excitations, where σ is expected to have the dependences given by equations (23).

For the present purpose, it is therefore convenient to express the thick target yield in terms of an effective target thickness dE_λ, which is measured in energy units and defined in such a way that equation (33) gives the correct value for the cross section corresponding to the energy E_0, if one makes the substitution

$$\frac{d\{Y\{n\}\}}{ds} \rightarrow \frac{Y\{n\}}{dE_\lambda} \cdot \frac{dE}{ds} \tag{39}$$

with all the quantities on the right-hand side taken at the energy E_0.

For bombarding energies in the region of interest for Coulomb excitation experiments, it seems that the stopping power dE/ds of almost all substances follows an energy dependence approximately proportional to the inverse square root of the energy of the projectiles (cf. Ma 2, Li 1). Employing such a relation one obtains, from (23), the effective target thickness

$$dE_\lambda = \frac{2}{3} E_0 \frac{\xi_0^{\frac{4\lambda}{3}-1}}{f_{E\lambda}\{\xi_0\}} \cdot \int_{\xi_0}^{\infty} \frac{f_{E\lambda}\{\xi\}}{\xi^{\frac{4\lambda}{3}}} d\xi, \tag{40}$$

where ξ_0 is the ξ-value (28) appropriate for the bombarding energy E_0. The values of dE_λ calculated from (40) are plotted in Fig. 9; they are rather insensitive to changes in the assumed energy dependence of the stopping power.

In the evaluation of the Coulomb excitation cross sections, we have employed the thicknesses given in the third column of Table I. The values have been determined in one of the ways

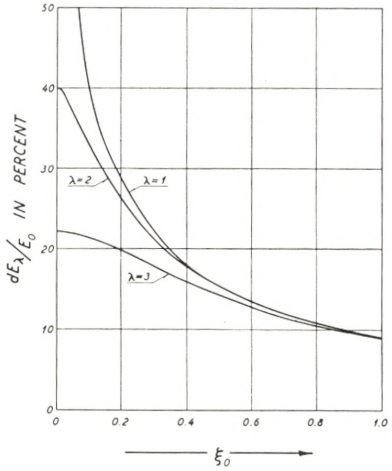

Fig. 9. Effective target thicknesses for $E\lambda$ Coulomb excitations, as defined by equation (40). The stopping power has been assumed to depend on the energy of the projectiles as $E^{-1/2}$, but the curves are rather independent of this assumption. The changes would be the largest for the small ξ_0-values, but even the assumption of an energy-independent stopping power would only increase the value for $\lambda = 2$ and $\xi_0 = 0$ from the 40 per cent given in the figure to a value of 50 per cent.

described above. The two methods with the profile curves and with the thick targets have been used in the majority of the cases and are the only ones which are expected to give reliable results.

IV. Results.

About three fifths of the elements with an odd number of protons have just one stable isotope, and the rest have no more than two. The results obtained with natural samples of these elements are therefore relatively simple to interpret. With five exceptions, of which only $_{71}Lu^{176}$ has a significant abundance

(2.6 per cent), all naturally occurring nuclides with an odd $Z \geqslant 9$ have an even number of neutrons and thus $I_0 \neq 0$. According to the considerations in Chapter II, one can therefore in general expect to excite the first two rotational states by the bombardment of these nuclides, and, in favourable instances, one should be able to detect three sets of conversion lines. It is of particular interest here to know the $K:L$ ratios of the $\Delta I = 1$

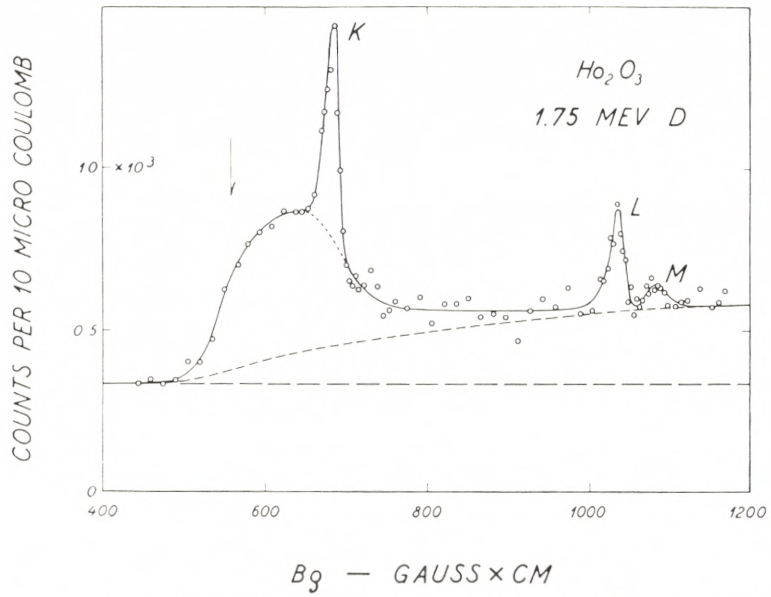

Fig. 10. Spectrum of internal conversion electrons from the K, L, and M shells of $_{67}Ho^{165}$ corresponding to the decay of the first rotational state. The excitations were produced by means of bombardment with 1.75 MeV deuterons, and the target contained 0.22 mg Ho per cm². The background consists of three parts. The first is field-independent and probably mainly produced by neutrons; the second is due to β-activities induced in light elements present in the target, and the third comes from the stopping electrons ejected from the holmium atoms (dotted peak). The latter two are cut-off at approximately 600 Gauss-cm, as an effect of the 1 mg/cm² mica foil covering the counter window.

decays, where the radiations will be of the mixed $M1$ and $E2$ type. As discussed earlier, under the present conditions, it is often easier to measure the K lines corresponding to the decays of the first rotational states, if one produces the excitations by means of bombardments with deuterons.

An example of a spectrum obtained with 1.75 MeV deuterons is shown in Fig. 10. Only one set of conversion lines is visible on

the spectrum; they correspond to the first excited state of the nuclide $_{67}Ho^{165}$, which has an isotope abundance of 100 per cent. The measured points scatter relatively much, because the deuterons induce a strong background of penetrating radiation (cf. Fig. 10), which fluctuates with the performance of the accelerator. The deuteron bombardments also produce β-activities in light atoms present in the targets and their supports. For this reason, the use of graphite or aluminum as support materials was excluded, and all the deuteron measurements have been carried out with targets prepared on a brass backing. On the other hand, it is also evident from Fig. 10 that the background of stopping electrons, to which the deuterons give rise, is sufficiently reduced to allow a relatively good measurement of the K peak; with proton bombardments, this peak only appeared as a hump on a much stronger background of stopping electrons.

Just as for Ho, most of the other odd-Z elements investigated proved to have first excited states which decayed predominantly through K conversion as a consequence of large $M1$ transition probabilities. For these elements, the measured excitation cross sections are not so reliable, since the determinations of the K line yields are rather dependent on the applied counter foil correction and the background conditions. For some of them, it was necessary to determine the K conversion yields from the measured L lines by employing K:L ratios known from other sources. For the even-even nuclides the situation is more favourable, since here the K lines are of relatively less importance.

The elements with an even Z often have three or more isotopes which are stable and comparatively abundant. Most frequently the mass numbers A are then also even and the ground state spin, consequently, $I_0 = 0$. For these nuclei, one cannot reach more than the first rotational state by an $E2$ excitation (cf. Chapt. II), and the decay will also have to be a pure $E2$ transition. Consequently the amount of K conversion is known theoretically (cf. Fig. 1), and since the coefficients in general are smaller than for the L shell, one can obtain rather reliable excitation cross sections from the measured L peaks, even if the K peaks are not measurable because of the background conditions.

Fig. 11 shows the spectrum of the L and M $(+N)$ peaks

measured for Er, where the first excited states of most of the even-even isotopes practically coincide. Another example, where this is not the case, is shown in Fig. 12. These two examples are typical of the even-Z elements also in that rather abundant odd-A isotopes are present in the natural samples. The L lines from the first rotational states of these isotopes will probably fall in the neighbourhood of those of the even ones. They will, however, be

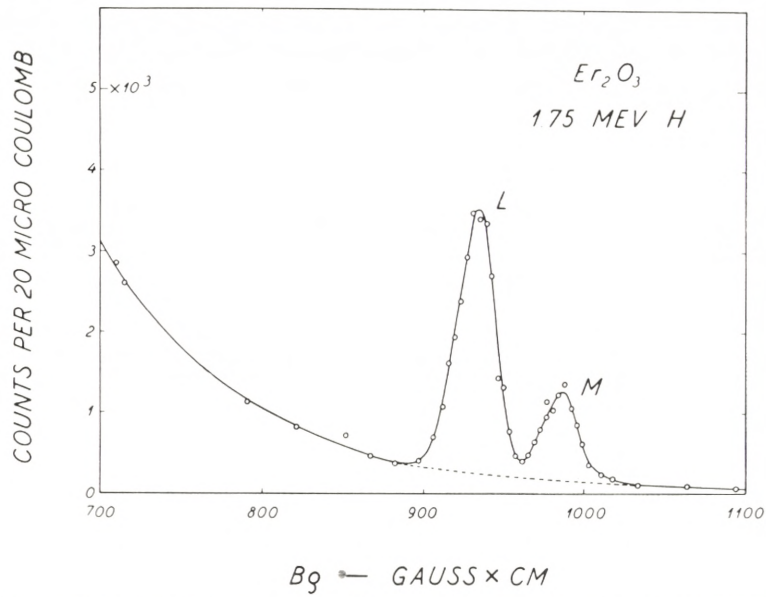

Fig. 11. The L and M (+ N) conversion peaks obtained by a 1.75 MeV proton bombardment of a target which contained 0.33 mg Er per cm². The transitions are assigned to the first excited states of the even erbium isotopes, which are supposed to have practically coincident excitation energies. The background is due to stopping electrons.

difficult to observe because of their relatively small intensities, which are a consequence partly of the smaller L conversion of the mixed transitions, and partly of the difference in the spin-weight factors appearing in the equations (7) and (8). Because of the comparatively small abundances it is also difficult to observe the very low lying K lines, and we have therefore in general disregarded the contributions from such isotopes. The situation may be different for elements such as W, where the odd isotope has a ground state spin $I_0 = 1/2$ and thus a rotational spectrum of the anomalous type (3).

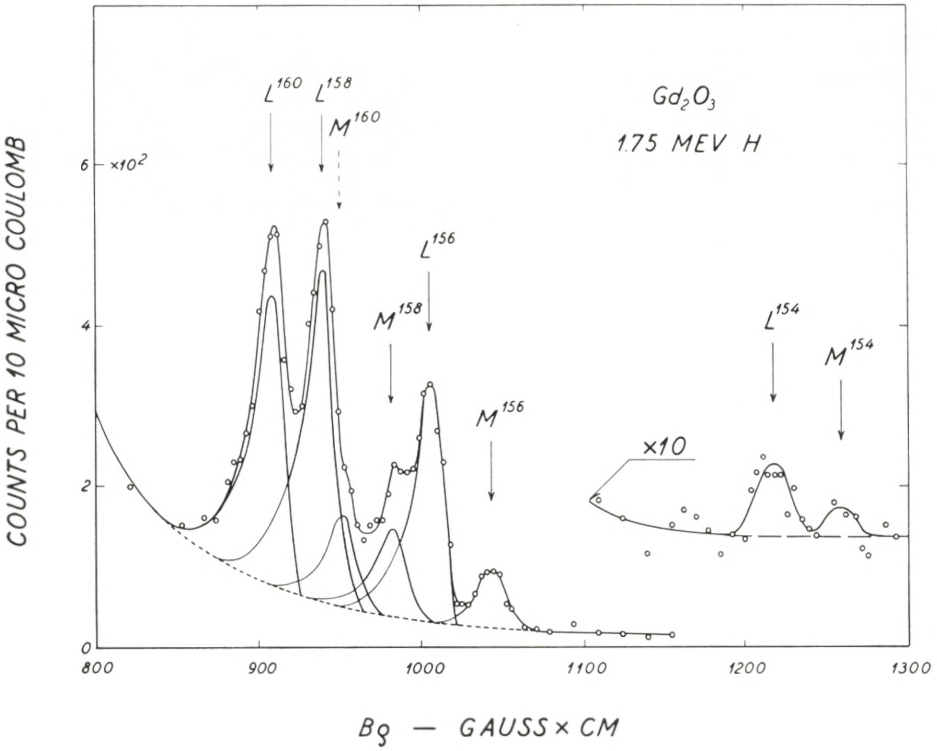

Fig. 12. Spectrum of conversion lines obtained by proton bombardment of a target which contained 0.26 mg Gd per cm². The peaks drawn indicate the contributions from the various isotopes, as assigned on the basis of the energy systematics (cf. the text).

Additional examples of the spectra discussed below are reproduced in previous publications (Hu 3, Bj 1).

In the Tables I and II, we have summarized the results which we have obtained so far from our investigations of a number of elements. In general, the spectra were only scanned for electron energies below 170 keV. The conversion lines found in the experiments have been assigned to the atomic shells of the various isotopes on the basis of the general systematics (cf., e. g., Bo 1), as well as by comparison with the information available from other experiments (cf., e. g., He 1, Mc 1, St 1, and Ho 1). From the measured peak areas we have computed the corresponding B-values by employing the natural isotope abundances given in the paper by HOLLANDER *et al.* (Ho 1). It has been assumed that all the excitations are of the $E2$ type, and that

the decays correspond to pure $E2$ transitions for the even-even nuclei, and mixed $M1 + E2$ transitions for the odd ones. In the following, we shall briefly comment on the transition energies and probabilities given in the tables. Our data can be compared with the results of the γ-measurements made by other investigators, but, in the present paper, we will only make a few remarks on those occasions in which major discrepancies are found. For a more detailed comparison between the various experimental results, the reader is referred to a forthcoming review article (Al 1).

---

25. MANGANESE. The thick target employed had been prepared by electro-plating. The surface was coloured and looked as if the manganese were covered with some sort of deposit; this may possibly imply that the value given in Table II for the excitation energy is somewhat too low. The main purpose of our Mn measurement was to demonstrate the extent to which the method of detecting the conversion electrons could be employed for lighter elements, and this element was known to have a large excitation cross section. Other investigators (Ma 1, Te 1) have measured a value of $0.07 \cdot 10^{-48}$ cm^4 for $\varepsilon \{\gamma_1\} B{:}e^2$, which, compared with the present result, indicates that the decay is a rather pure $M1$ transition. Thus, a $Q_0 \simeq 1$ barn would be found if the excitations were interpreted as rotational.

26. IRON. A thick target consisting of iron enriched about 20 times in Fe^{57} was employed for the measurements. We found two lines which we assigned to this isotope because of the good agreement with the conversion lines seen in the decay of $_{27}Co^{57}$ (cf. Al 3). Due to the 50 per cent content of other Fe-isotopes in the target, the signal to noise ratio was comparatively small, and the $L + M$ lines were not measurable. However, the $K{:}L$ ratio is not either a good measure of the mixing, since it is about equal for the $M1$ and $E2$ transitions in this region. The multipolarity can be determined much better from the α_K coefficients (cf. Al 3), which show that the 122 keV decay corresponds to a nearly pure $M1$ transition, whereas the 137 keV decay is of the $E2$ type. From the measured partial B-values one

can therefore determine the branching fractions, β, for the transitions to the ground state and to the first excited state at about 14 keV, respectively, as well as the total B-value for the second excited state. The multipolarities found for the transitions evidently conform with those corresponding to a normal rotational spin sequence 1/2, 3/2, 5/2, for which the data would yield the Q_0-value given in Table II.

47. SILVER. The K lines corresponding to the lowest collective excitation in each isotope could barely be measured, and those corresponding to the cross-over and stop-over transitions from the next collective state around 410 keV were not detectable. Large uncertainties must be ascribed to the total B-values obtained. More reliable results can be derived from the γ-ray measurements (cf. He 2, St 1, Mc 2). The level schemes for the silver isotopes have been discussed briefly elsewhere (Hu 2) on the assumption that the excitations may be described in terms of rotational states.

58. CERIUM. No lines were found in the investigation.

59. PRASEODYMIUM. No lines were found in the investigation.

60. NEODYMIUM. The two weak lines found were assigned to a low-lying first excited state in the heavy isotope Nd^{150}, which has an abundance of less than 6 per cent. The assignment was made because it was known that the higher mass numbers in this region correspond to the lower excitation energies (Bo 1). Recent γ-measurements on separated targets (He 1, Si 1) show that the assignment is correct and that the estimated B-values are approximately right. In the case of Nd, the measurements have not been repeated with sprayed targets, while this has been done for all the following elements of the rare earths.

62. SAMARIUM. With this element the region of strongly deformed nuclei is approached and the excitation cross sections become correspondingly large. Unfortunately, the K_1 line of Sm^{152} appears to coincide with an L_1 line of Sm^{154}. The yield of the composite peak depends on the bombarding energy in a way which indicates that most of it is due to L conversions. The fraction which corresponds to K conversion has been estimated

from the yield of the L_1 line of Sm^{152} by means of the $K:L$ ratios given in Fig. 2. In the same way we can then calculate the yield which should be expected for the K_1 line of Sm^{154}. However, the energy for these electrons is only about 36 keV and they are therefore difficult to observe. Deuteron measurements made at an early stage did not give any clear evidence for the expected peak. From our data we estimate partial B-values for γ-emission, which are 0.7 and 2.0 times those obtained for Sm^{152} and Sm^{154}, respectively, through direct measurements of the emitted γ-rays (He 1).

63. EUROPIUM. The two most important peaks in the spectrum were interpreted as the L_1 and K_2 lines of the 52 per cent abundant isotope Eu^{153}, because the other stable isotope Eu^{151} has less than 90 neutrons and is therefore expected to have appreciably higher excitation energies (cf. Bo 1); that this is the correct interpretation follows moreover from recent γ-coincidence measurements and β-decay evidence (cf. He 1, Ma 3). Thus, we obtain a value of 2.30 for the ratio between the excitation energies of the second and first excited states, in good agreement with the value corresponding to rotational excitations of a nucleus with $I_0 = 5/2$ (cf. Eq. (5)). Our absolute values for the excitation energies seem, however, to be somewhat higher than found in the γ-ray measurements. Our earlier deuteron measurements indicate that $K:L \sim 1$ for the decay of the first excited state, and with this value for the ratio B-values consistent with the nuclear theory are obtained by means of the formulae (16) to (21). Although the indications of a peak corresponding to the expected stop-over L_{21} line also fits into the picture, it is still only a very crude determination of the $M1$ contributions, as the yield of the weak K_2 line is rather uncertain. However, the fact that this line is observed shows clearly that the $M1$ transition probabilities must be relatively small. Comparison with the partial B-value found for the corresponding γ-ray (He 1) indicates that the cross-over transitions should actually be even stronger than we have found.

64. GADOLINIUM. Evidently there is some ambiguity in the way in which the yield corresponding to the large group of peaks in Fig. 12 has been divided among the various L and M

lines, which are only partly resolved from each other. On the whole, the curves shown correspond to $(M+N):L$ ratios which are somewhat lower than those given in Fig. 2. However, the computed B-values agree well with the recent results obtained from γ-measurements (He 1), except for the isolated, but very weak $L_1{}^{154}$ line. From our data we estimate a partial B-value for the γ-emission corresponding to this line, which is about 1.8 times smaller than that found directly. Higher energy radiations from the odd Gd-isotopes have been observed in the same γ-experiments, but with the yields reported, we would not be able to detect the corresponding conversion lines. (Cf. also the discussion in the beginning of the present chapter).

65. TERBIUM. The only terbium line which could be detected with certainty was the L_1 line at 49 keV. From the yield of this line alone it is not possible to determine the total B-value, as it does not give the magnitude of the mixing ratio. However, on the basis of the rotational description, one would expect the nucleus to have a second excited state at approximately 139 keV (cf. Eq. (5)), and the fact that the corresponding transitions to the ground state did not give any detectable conversion lines, implies that the cascade transitions must be the strongest, and thus predominantly of the $M1$ type. We find that more than 80 per cent, and probably as much as 90 per cent, of the L_1 peak must be due to $M1$ transitions. Consequently, it ought to be possible to detect the cascade lines, even though the background is higher at the lower energies; unfortunately, however, all the terbium samples available were more or less contaminated with dysprosium, and the comparatively strong lines from this element concealed the presence of the stop-over lines. However, the data seem consistent with the mentioned degree of mixing. Recently, HEYDENBURG and TEMMER (He 1) have succeeded in measuring the γ-rays from the cross-over transitions. They find an energy of 136 keV and a yield which is about 1.6 times larger than that which we estimate on the basis of the above assumption.

66. DYSPROSIUM. The two strong transitions observed are assigned to the two most abundant even isotopes on the basis of the energy systematics found in this region of the elements.

From the data we estimate partial B-values for γ-emission which are about 1.5 times larger than the values measured directly (He 1). From the arguments given in the introduction to this chapter it is not expected that the odd Dy isotopes would give rise to any measurable intensities, and no lines corresponding to these nuclei were observed.

67. HOLMIUM. This element provides a typical example, showing the ways in which one can test some of the regularities predicted by the theory. The only stable isotope of holmium is Ho^{165}. The L electrons corresponding to the first excited state of this nucleus were easily measured in the proton experiments, but for the K line it turned out that the best results were obtained from deuteron bombardments. From the measured $K:L$ ratio for these transitions we determine the branching and mixing ratios for the transitions from the second excited state, as computed by means of the formulae (16) to (21). In the proton measurements we also found a weak line corresponding to the L_{21} transitions and we can therefore calculate the total B-values for both states. The experimental results are seen to be consistent with the rotational description, which predicts an energy ratio of 20:9 and a ratio for the B-values of 35:9, whereas the measured ratios are 2.21 and $\simeq$ 3.2, respectively. In addition, the indications of K conversion peaks from the decays of the second excited state have estimated intensities in agreement with the theoretical expectations. It must, however, be admitted that the transition probabilities given for the second excited state are computed on the basis of very uncertain yield measurements. It is therefore not surprising that our estimate of the partial B-value for the cross-over γ-ray is about two times larger than the value obtained directly from the γ-measurements (He 1). This indicates that the $M1$ transitions are even stronger than those corresponding to the mixing ratios given in Table II, but this would only be of minor importance for the total B-value computed for the first excited state.

68. ERBIUM. The masses of the erbium isotopes fall in the middle of the region where the energies for the first excited states of the even-even nuclides change only slowly with the mass num-

ber. The excitation energies can consequently be expected to be practically the same for all the even Er isotopes, and to these nuclei we therefore assign the pair of conversion lines shown in Fig. 11. The coincidence between the excitation energies is evidently complete within the limits of the experimental resolution. As for most other even-Z nuclides we do not find the lines from the odd-A isotopes.

69. THULIUM. The spin of the only stable thulium isotope Tm^{169} is known to be 1/2 (cf., e. g., Li 2), and one can therefore expect to find the anomalous rotational spectrum given by formula (3). The strongest Coulomb excited line in both the conversion electron and the γ-ray measurements (He 1) corresponds to a transition energy of approximately 110 keV. The peak found at the position of the M line from this transition appeared too strong relative to the L line to be a pure M peak, and the clear indication of a peak, which was found at a slightly higher energy, also supports the impression that additional transitions are present, corresponding to an energy about 119 keV. Relative to the L peak, the composite peak does not appear to be weaker at the lower proton energies, and we are therefore led to an assignment in which the two transitions belong to a 119 keV excited state, decaying mainly via the stop-over to a first excited state at about 8 keV, but also to some extent by the cross-over to the ground state. As a check, we have measured the excitation function for the 110 keV transitions; it was found to conform with an excitation energy of about 120 keV, even though the evidence was not quite conclusive. In addition, the above interpretation seems to be consistent with recent β-decay experiments (Jo 1).

For a normal spin sequence the assumed level scheme leads to the value $a = 0.79$ for the decoupling parameter in equation (3), and a moment of inertia which would correspond to an energy of $6\,\hbar^2/2\Im \simeq 75$ keV for a first excited state in a similar even-even nucleus. These values are in good accord with recent theoretical estimates (Mo 1). The measured yields show that the presumed stop-over lines correspond to rather pure $M1$ transitions, put the $K{:}L$ ratio is so large that only an upper limit to the cross-over branching fraction can be obtained in this way. Instead, we have determined this quantity directly by comparison with the

measured cross-over yield, and Table II therefore contains only one value for the total transition probability.

70. YTTERBIUM. The situation here is completely similar to that of erbium, and the remarks made there apply also to the ytterbium measurements. In addition, we found in the α-bombardement of Yb a weak indication of a peak in the spectrum at an energy around 57 keV. If the peak is real it is most probably an L peak associated with a 66 keV transition, but we have no basis for further assignment.

71. LUTECIUM. The only conversion lines we detected with certainty were those from the decay of the first excited state of the 97 per cent abundant isotope Lu^{175}. The measured $K:L$ ratio shows that the majority of the decays correspond to $M1$ transitions, indicating that cross-over transitions from the expected second rotational state should be comparatively weak. The corresponding γ-ray has been observed in the experiments of HEYDENBURG and TEMMER (He 1), who find the ratio between the excitation energies to agree well with the theoretical value. On the basis of our data, we estimate a partial B-value for the cross-over γ-ray, which is about 4 times larger than the value found directly in the above mentioned γ-measurements. However, our value for the mixing ratio is derived from equation (20) and depends critically on the $K:L$ ratio, which only has to be decreased by 20 per cent in order to remove the apparent discrepancy. This change would only be of minor importance for the computed total B-value for the first excited state, which is also found to be in good agreement with the results obtained by the above experimentors. On the other hand, for $|g_K - g_R|$, it would imply that the correct value should be approximately 1.8 times smaller than given in Table II. The yields which should be expected for the conversion lines associated with the decay of the second excited state are so small relative to the respective backgrounds that they would only be measurable under improved experimental conditions.

72. HAFNIUM. Our measurements on this element have so far only been made by bombardment of a comparatively thick HfO_2 target, which had been prepared by the suspension method. When viewed in a microscope after the bombardment, the target

layer appeared to consist of rather small grains which were evenly distributed and which covered approximately 90 per cent of the surface. The thickness determination by means of weighing should therefore not be so bad in the present case.

In hafnium, the odd-A isotopes have excitation energies for the first rotational state, which are higher than those for the even ones. In spite of their comparatively small intensities, it was therefore also possible to detect the L conversion lines for the odd isotopes. The corresponding K lines were too weak to be measurable, but indications gave estimated $K{:}L$ ratios of the order of 2. This ratio would correspond to partial B-values for γ-emission, which agree reasonably well with the γ-ray measurements (He 1, St 1, Mc 1). However, for Hf^{177} the transition from the first excited state has been reported (Ma 4) to have $\delta^2 \lesssim 0.02$, and it is by employing this value that the very low B-value given in Table II has been computed. We have assumed that $I_0 = 7/2$ in agreement with the observed rotational energy intervals (cf. He 1), but this is of minor importance for the computed transition probabilities. For the even isotopes, a similar comparison with the γ-ray measurements is less uncertain and the measured intensities are found to agree approximately with each other. The target was relatively thick and therefore the resolution obtained was not very good. Only in the α-particle bombardments could the weak Hf^{176} lines be detected simultaneously with those from the more abundant isotopes, and this was because of the better resolution which was obtained as a consequence of the smaller effective target thickness. Comparison with the γ-ray measurements made with separated targets (Mc 1, He 1) shows that all our energy determinations for the hafnium lines are 1 or 2 keV too high, but that the assignments made are correct.*

73. TANTALUM. The Ta^{181} nucleus is one of those for which more detailed studies have been made by means of Coulomb excitation experiments, and in several papers the results have been discussed in terms of the rotational interpretation (cf., e. g., Bo 5). All three γ-rays from the excitation of the two lowest

* Note added in proof. Repeated measurements on sprayed targets have yielded partial B-values which are somewhat smaller than those given in Table I. For the $L_1^{178,\,180}$ peak, the average is $2.3 \cdot 10^{-48}$ cm^4, corresponding to a quadrupole moment $Q_0 = 7.0$ barn.

excited states have been detected, and coincidence experiments as well as angular distribution measurements have confirmed that the energy ratio and the spin sequence for the levels are as predicted for a rotational spectrum.

The energies given in Table II are, as mentioned earlier, calibrated against the 100 keV transitions found for excited W; the values are slightly lower than those published earlier (Hu 3, Hu 1), but the ratio is still found to be 2.21 in excellent agreement with the theory. If we add all the partial B-values which we have measured for the first rotational state and, by means of equations (7) and (8), compare this total with the partial B-value measured for the practically unconverted cross-over γ-transitions from the second state, then we find that one should expect that 80 per cent of the transitions from the second level have decayed via the cascade to the first level. This means that $\delta^2 \simeq 0.14$ or that the cascade transitions are practically pure $M1$ decays in agreement with the measured conversion coefficients, as well as with the angular distribution measurements of McGowan (Mc 3). With these values for the branching and the mixing ratio we can determine the total B-value for the second excited state from the measured stop-over conversion lines and thus obtain a practically independent check on the branching fraction. The total B-value is found to be 3.6 times smaller than for the first excited state, in excellent agreement with the theory. This is of course somewhat coincidental, since the yield of the stop-over conversion lines are not very accurately measured, but, nevertheless, it gives a relatively good confirmation of the values for the branching fractions, and therefore also of the determination of the mixing ratio and $|g_K - g_R|$.

74. TUNGSTEN. With targets of natural tungsten there are several coincidences in the position of the conversion lines from the various isotopes. In bombardments with α-particles of sufficiently low energy the only lines which remained were those corresponding to the low-lying first excited state of W^{183}. The $M + N$ peak from the decay of this level was easier to measure than the L peak, as the background was much higher for the latter peak which, moreover, was very close to the foil cut-off. The conversion coefficients are known from the β-decay work

of MURRAY *et al.* (Mu 1). Using their results we can compute the total B-value from the M peak alone, if we look apart from the fact that our $L:(M+N)$ ratio seems too low. The computed B-value is however rather uncertain, and we have therefore repeated the experiment with a sprayed target made of WO_3 enriched in W^{183}. These measurements confirm that the transitions take place in the odd isotope; unfortunately, however, we cannot evaluate a reliable transition probability from the data until information on the isotopic composition of the target material becomes available. The spin of W^{183} is 1/2 and the second excited collective state is found to have an energy of 99.1 keV (Mu 1, Mc 4). This is 2.13 times the excitation energy for the first collective state and corresponds to $a = 0.19$ and $3\,\hbar^2/\Im = 78$ keV, which is in good accord with theoretical expectations (Mo 2, Ke 1). The excitation energy for the first excited state in the even isotope W^{182} is 100.1 keV (cf. Bo 3), which is very close to the value for the second excited state of the odd isotope. We cannot expect to be able to discriminate between these two $E2$ transitions in our measurements and, for this reason, we cannot determine the yield corresponding to the second excited state in W^{183}, or the amount of W^{182} in the enriched target. For the natural targets, the yield of the composite L peak will be due mainly to the even isotope, for which one can therefore obtain a rather reliable B-value determination. For the measured peak we estimate the W^{183} contributions to be about 20 per cent, if we assume that $Q_0 = 6.5$ barns (as interpolated from Fig. 13) rather than the uncertain 8.4 barns given in Table II.

Also for the other two even isotopes, coincidences of the positions of the M and L conversion peaks make an accurate comparison of the total B-values difficult, as we have to employ the relative conversion coefficients given in Fig. 2. The average value computed for all the even isotopes corresponds to a partial B-value for γ-emission, which is in good agreement with our previously published measurements (Hu 1), and with those of STELSON and MCGOWAN (St. 1).

The value found in the experiments of MCCLELLAND *et al.* (Mc 1) is about three times smaller; their measurements on separated targets have confirmed the assignments given in Table I (cf. Mc 4).

75. RHENIUM. The pure metal of this element was only available in the form of a powder consisting of comparatively large grains. Consequently, our earlier experiments made with targets prepared by the suspension method were not very reliable, and we have therefore repeated the measurements with sprayed targets. In addition to the group of L and M lines from the decay of the first excited state of each of the two stable isotopes Re^{185} and Re^{187}, the spectrum also showed the corresponding K line associated with the latter nuclide. The $K:L$ ratio thus obtained is in good agreement with the value found from measurements on the β-decay of $_{76}Os^{187}$ (cf. Ho 1). For Re^{187} we can therefore compute the total B-value in the usual way; the corresponding value for γ-emission turns out to be about two times larger than that obtained directly in the experiments of McClelland *et al.* The K line associated with Re^{185} could not be detected with certainty, but the indications are that the $K:L$ ratio is lower than for Re^{187}. For the lighter isotope the ratio is not known from other sources, and we have therefore only given the two limits for the total B-value, which correspond to either a pure $M1$ or a pure $E2$ decay.

76. OSMIUM. Many small peaks were seen in the measured spectrum, but they were all of the same magnitude as the experimental fluctuations in the background and no lines were established with certainty.

77. IRIDIUM. The spectrum measured for this element is very similar to that obtained in the bombardment of rhenium. The measurements were made with a thick target of the pure metal, but the L peaks from the de-excitation of the two stable isotopes were clearly resolved due to the fact that the layer corresponding to the effective target thickness is comparatively thin for electrons with energies above 100 keV. The determination of the yield of the measured M peak was rather uncertain and we only found weaker indications for the K peaks. The $K:L$ ratios for the two levels are however known from β-decay experiments (Ho 1, Wa 1), and we can thus compute the B-values and the corresponding moments in the usual way.

78. PLATINUM. Bombardment of a thick target of pure platinum metal yielded only two weak lines; they correspond

to the energies for the K and L electrons from a 210 keV decay. This transition has previously been found by McCLELLAND *et al.* (Mc 1), and by TEMMER *et al.* (Te 1). By means of separated targets the former authors have shown that the process takes place in Pt^{195}. This nucleus is of the even-Z odd-A type, and has a spin $I_0 = 1/2$. The L peak was barely visible, but the $K:L$ ratio is definitely so large that the decay must be mainly $M1$, and the level therefore has $I = 3/2$.

79. GOLD. For this element the deviation from the spherically symmetric form of the closed-shell nuclei has become so small, that, in the present experiment, it was difficult to detect the Coulomb excitation of the collective states. These states, however, have been investigated in detail by the γ-ray technique, and angular distribution measurements have shown that $\delta^2 \lesssim 0.6$ for the first excited state at 279 keV (cf. Mc 3). With this value for the mixing ratio we have computed the total B-value from the estimated size of the K peak.

92. URANIUM. After having replaced the Geiger counter with an anthracene detector we looked for the L conversion line from the decay of the 44 keV first excited state in U^{238}. However, the background of stopping electrons was so strong at these low energies that the line could not be detected with certainty.

The partial B-values for γ-emission, which we estimate from our data by means of the conversion coefficients given in Figs. 1 and 2, are on the whole in satisfactory agreement with the results obtained from the γ-ray experiments. On the average, the deviations seem to be about 25 per cent, and this is of the same order of magnitude as the experimental uncertainties.

An additional check on the experiments, which at the same time constitutes a test of the theory of Coulomb excitation, can be obtained by computing the reduced transition probabilities for the excitations from the directly measured lifetimes of the excited states. As mentioned in Chapter II, such a comparison is independent of any particular nuclear model, but it demands a rather good knowledge of the magnitude of the various conversion coefficients (cf. Eq. (31)), because the $E2$ γ-transitions

often constitute only a small fraction of the decays. However, the above mentioned agreement between the conversion electron and γ-ray measurements indicates that the applied conversion coefficients are approximately correct, and the comparison should therefore be a significant test of the theory of the excitation process.

The half-lives for the decays of the first excited state of several of the even-even nuclei in which we are interested here have been measured in recent years (cf. Su 1), and these transitions are particularly well suited for comparison, because they have no magnetic contributions. In Table III, we have given the values for the half-lives as well as the corresponding reduced transition probabilities, corrected for the spin weight factors so that they can be compared directly with the B-values of Table II (cf. Eq. (30)). The approximate agreement between the B-values obtained by the two different kinds of experiments seems very satisfactory when one considers all the uncertainties involved. A similar result has been obtained by HEYDENBURG and TEMMER (He 1), who have compared their data with the lifetimes by means of total conversion coefficients taken from the paper of SUNYAR. The values of $\varepsilon\{\gamma\}$, which we have employed in Table III, deviate by less than 10 per cent from those given by SUNYAR.

V. Discussion.

From the experimental results summarized in Table II, one can compute the nuclear moments and gyromagnetic ratios by means of the formulae given in Chapter II, on the assumption that the observed excitations are of rotational character. This interpretation is suggested by the large electric quadrupole transition probabilities characterizing the excitations, as well as by the systematic trends in the properties of the observed levels (cf. below). For a few of the odd-A nuclei where two excitations could be observed (Eu, Ho, and Ta), the predictions of the theory have also been tested, in a more quantitative way, by the measured ratios of the energies and excitation cross sections for the two levels. As far as the relative cross sections are concerned,

the consistency of experiment and theory is evident from the approximate equality of the Q_0-values derived from the excitations of the two levels (cf. Table II).

A. Quadrupole Moments.

The Q_0-values obtained from the present measurements and listed in Table II are plotted in Fig. 13 as a function of the nuclear mass number A_2. They exhibit a rather smooth variation, with fluctuations not exceeding the experimental uncertainties.

These intrinsic quadrupole moments may be compared with those derived from spectroscopic measurements for odd-A nuclei, by means of the relation (9). Previous comparisons of this type (cf., e. g., Bo 4) indicated that the latter Q_0-values somewhat exceed those derived from transition probabilities. However, for $_{71}Lu^{175}$ and $_{73}Ta^{181}$, where the discrepancies were largest, a

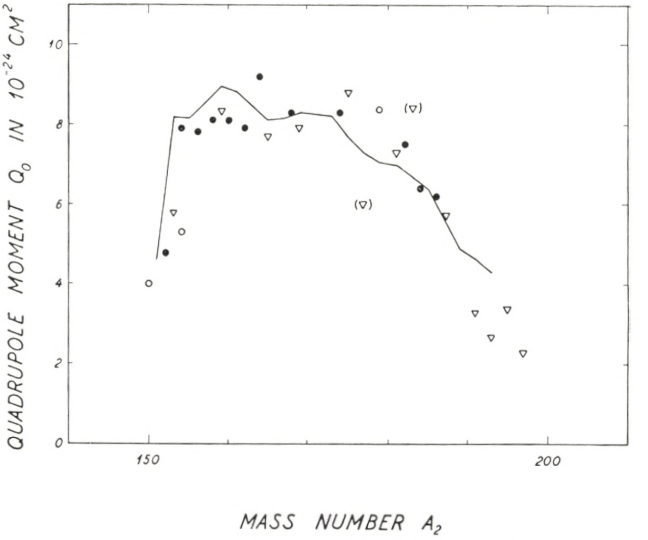

Fig. 13. The Q_0-values given in Table II plotted as a function of the mass number A_2.* The circles represent the even-A nuclides and the triangles the odd-A nuclides. The uncertainties are supposed to be of the order of 10 % for the black points, and 20 % or more for the rest of the points. The points in parentheses correspond to $_{72}Hf^{177}$ and $_{74}W^{183}$, (cf. the comments in Chapt. IV). The broken line represents the theoretical moments for the odd-A nuclides, corresponding to $r_0 = 1.20 \cdot 10^{-13}$ cm (cf. Mo 1).

* Cf. footnote p. 45.

recent more detailed analysis of the electronic configurations has led to a considerable decrease in the spectroscopic Q-values (Ka 1). For $_{71}Lu^{175}$ and $_{73}Ta^{181}$ the revised spectroscopic analysis yields Q_0-values of about 12 barns and 9 barns, respectively, to be compared with the values 9 barns and 7 barns, listed in Table II. The remaining deviation is hardly significant, in view of the existing experimental uncertainties.

Recently, a theoretical estimate of nuclear quadrupole moments has been made on the basis of the calculation of the binding energies for individual nucleons in deformed potentials (Mo 1). The equilibrium deformation has been determined by minimizing the total energy of the system of nucleons. The quadrupole moments, calculated in this way for the odd-A nuclei between $A_2 = 151$ and $A_2 = 193$, are shown in Fig. 13, where the theoretical points are connected by a broken line. The absolute magnitudes correspond to the value $r_0 = 1.20 \cdot 10^{-13}$ cm. The agreement is very satisfactory, except for $_{73}Eu^{153}$, where our experimental quadrupole moment is about 30 per cent lower than the theoretical Q_0-value.

B. Moments of Inertia.

The nuclear moments of inertia $\Im$ derived from the observed excitation energies by means of equations (1) or (3) show a similar variation with A_2 as the quadrupole moments, with a broad maximum in the region around $A_2 = 170$.

Of special interest, from a theoretical point of view, is the relation between the moments of inertia and the nuclear deformations. This is illustrated by Fig. 14, where the $\Im$-values determined from the energies given in Table II are plotted against Q_0. The correlation of the two quantities is evident from the grouping of the points around the dashed line shown in the figure, with the largest deviation from the general trend again occurring for $_{63}Eu^{153}$. For comparison, the $\Im$-values calculated from the relation (11), corresponding to the assumption of irrotational flow for the rotational motion, are also shown in the figure. It is seen that such a model gives moments of inertia which are smaller than the observed moments by factors of more than four, as has also been recognized previously (Bo 1, Fo 1, Su 1).

The relation (11) assumes a simple ellipsoidal nuclear shape, and an increase of the moments of inertia for the irrotational model could arise from the occurrence of higher multipoles in the shape. It appears, however, (Gu 1) that while such an effect is not unexpected and may have an appreciable influence on the moment of inertia, the ratio of $\Im$ and Q_0^2 is much less affected.

A recent analysis of the nuclear rotational motion (Bo 2) has also shown that important deviations from irrotational flow

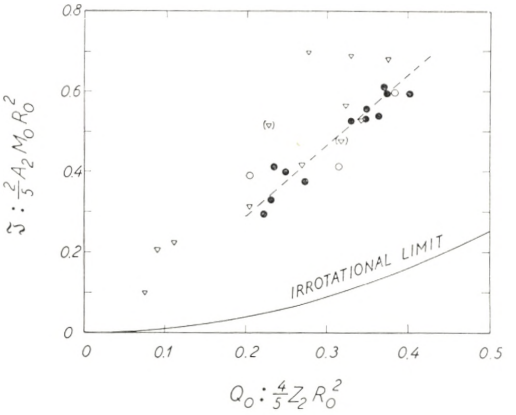

Fig. 14. Moments of inertia determined from the excitation energies by means of equations (1) or (3), and plotted against the corresponding nuclear deformations, as represented by the Q_0-values (cf. Table II).* For the average nuclear radius we have employed the value $R_0 = r_0 \cdot A_2^{1/3}$, with $r_0 = 1.20 \cdot 10^{-13}$ cm. A correlation between the two quantities is indicated by the grouping of the points around the broken line. The points are marked in the same way as in Fig. 13.

are to be expected as a consequence of the nuclear shell structure. Thus, it is found that for pure independent particle motion in a deformed potential, the moment would be approximately equal to that for rigid rotation. The effect of residual interactions between the particles, not included in the average nuclear field, results in smaller moments of inertia, which increase with increasing deformation. The values for irrotational flow are approached when the interactions become so strong that they destroy the shell structure. The observed magnitude and trend of the moments of inertia are interpreted as indicating a strength of interaction about three times smaller than corresponding to this limit (Bo 2).

* Cf. footnote p. 45.

C. Magnetic Moments.

The $M1$ transition probabilities are measures of the quantities $|g_K - g_R|$ (cf. Table II), and if, in addition, the magnetic moments of the ground states are known, the values of the two gyromagnetic ratios can be determined separately by means of equation (12). However, the ambiguity in the sign of $(g_K - g_R)$ implies that two sets of g-values come into consideration. When the experimental data are uncertain, one is therefore left with a very large range of possible g-values, and only little can be learned from the measurements. This applies to most of the elements considered here, with the exception of the nuclei $_{63}Eu^{153}$ and $_{73}Ta^{181}$. For the former, the occurrence of the comparatively strong cross-over transitions shows that the magnetic transitions must be weak, and consequently the gyromagnetic ratios g_K and g_R must be approximately equal. From spectroscopic evidence the magnetic moment is known to be about 1.6 n. m., which corresponds to the values $g_K \simeq g_R \simeq 0.64 \pm 0.1$, whereas the estimate (14) yields a value of $g_R \simeq 0.41$. As mentioned in the comments on $_{73}Ta^{181}$, one has for this nucleus a comparatively good determination of the magnetic transition probabilites, which, by means of the value $g_R = 0.40$ estimated from (14), yields the magnetic moments 0.1 n.m. or 2.9 n.m. for the ground state. The former of these values is excluded by the angular distribution measurements (Mc 3) which show that $(g_K - g_R)$ is positive if Q_0 is positive (cf. Chapter II A), as is indicated by the spectroscopic Q-values. The spectroscopically determined magnetic moment is 2.1 n.m. (Br. 2), and combined with our data this value would correspond to $g_R = 0.17$.

In order to obtain more information about the gyromagnetic ratios, better measurements of both the magnetic moments and the transition probabilities are needed. The present measurements have shown that, in general, the magnetic transition probabilities are large, and this implies, as mentioned in Chapter II, that they are best determined by direct measurements of the branching fractions for the second excited states. One should, thus, compare the yield of the cross-over γ-rays with the yield of the cascade conversion lines. Reliable measurements of the latter demand a better experimental technique than the one

employed in the present work. It would probably be advantageous to monitor the electron yields by means of the elastically scattered projectiles, and to stabilize the position of the beam so that a higher resolution could be employed in the β-spectrometer. This would also improve the accuracy in the measurements of the yields in the decays of the first excited states, since the movements of the beam are responsible for the uncertainty in the determination of the half-widths and peak areas of the measured lines. Further improvements would imply the use of thin-walled counters and evaporated or painted (Gl 1) targets, as well as considerations of the angular distributions of the conversion electrons. We hope to be able to investigate some of the more interesting nuclei in this manner, when the new 4-MeV electrostatic generator of this Institute comes into regular operation.

In conclusion, we want to express our gratitude to Professor NIELS BOHR for his continued interest in our work and for the excellent working conditions offered at his institute. In addition, we would like to thank Drs. A. BOHR and B. R. MOTTELSON for much advice and for great help in the attempts to interpret the obtained data. We are also grateful to cand. mag. B. S. MADSEN for his aid with the electronic equipment and for his assistance in some of the experiments. Finally, we gratefully acknowledge the kindness by which many samples of the rare earth oxides have been put at our disposal by various institutions, in particular by the 'Iowa State College', Iowa City, U.S.A., and by 'Chalmers Tekniska Högskola', Göteborg, Sweden.

Appendix I.

The non-relativistic theory for the ionization of the K shell by bombardment with heavy particles has been treated by HENNEBERG (He 3) on the basis of the Born approximation. For the present purpose, it is of interest to extend these calculations to include also the higher shells, and we shall therefore briefly outline a simple derivation of Henneberg's formula.

In the evaluation of the matrix elements one is, according to HENNEBERG (l. c.), justified in employing the Born approximation, i. e., to replace the product of the initial and final wave functions for the bombarding particle by the product of two plane waves, and this is true because the radii of the electron orbits are large compared to the classical distance of closest approach for the projectiles. With such a substitution, the integration over the coordinates of the bombarding particle is straightforward, and one obtains (cf. Be 1) the following expression for the differential cross section for the emission of an electron of energy E_δ:

$$\frac{d\sigma}{dE_\delta} \simeq 4\,\pi Z_1{}^2 \frac{M_1}{E_1}\frac{e^4}{\hbar^2}\int_{q_{\min}}^{\infty} |V\{q\}|^2 \frac{dq}{q^3} \qquad (43)^*$$

$$V\{q\} \equiv \int e^{i\vec{q}\cdot\vec{r}} \cdot \psi_f{}^*\{\vec{r}\} \cdot \psi_i\{\vec{r}\}\, d\vec{r}\,, \qquad (44)$$

where $Z_1 \cdot e$, M_1, and E_1 are the charge, mass, and energy of the bombarding particle which has suffered a momentum change $\hbar\vec{q}$ in the C. M. system. From the conservation of energy and momentum, it follows that

$$\hbar q_{\min} \simeq (E_B + E_\delta) \cdot \sqrt{\frac{M_1}{2E_1}}, \qquad (45)$$

where E_B is the actual binding energy of the ejected electron. Consequently, $\exp\{i\vec{q}\cdot\vec{r}\}$ will be a rapidly varying function as compared to the electron wave functions ψ, provided that one or both of the following two conditions are fulfilled:

$$E_B > E_0 \text{ or } E_\delta > E_0, \qquad (46)$$

where E_0 is the maximum energy which an electron can obtain in a free collision with the bombarding particle, i. e.

$$E_0 \simeq 4\,m\frac{E_1}{M_1}, \qquad (47)$$

if 'm' denotes the electron mass.

Provided that the condition (46) holds, one can easily show, by expanding $\exp\{i\vec{q}\cdot\vec{r}\}$ in spherical harmonics and performing repeated partial integrations, that, to leading order in $1/q$, only

* N. B.: Formulae numbers 41 and 42 are omitted.

s-states contribute to the integral V. For these states one obtains in the same way

$$V_s = \int_0^\infty \frac{\sin\{qr\}}{qr} \cdot R_{sf}\{r\} \cdot R_{si}\{r\} \cdot r^2 \cdot dr \simeq -\frac{2}{q^4}\left[\frac{d}{dr}(R_{sf} \cdot R_{si})\right]_{r=0} \quad (48)$$

or, from the differential equation for the radial wave functions R_s,

$$|V_s|^2 \simeq \frac{2^4}{q^8}\left(\frac{Z_2}{a_0}\right)^2 \cdot |R_{sf}\{0\}|^2 \cdot |R_{si}\{0\}|^2, \quad (49)$$

where $Z_2 e$ is the charge of the target nuclei and a_0 the Bohr radius of the hydrogen atom.

If one neglects screening effects, one has (cf., e. g., SOMMERFELD (So 1)) for the n^{th} shell

$$|R_{si}\{0\}|^2 = 2^2 \cdot \left(\frac{Z_2}{n\, a_0}\right)^3 \quad (50)$$

and

$$|R_{sf}\{0\}|^2 = 2^2 \frac{m}{\hbar^2}\frac{Z_2}{a_0}\left[1 - \exp.\left\{-2\pi \frac{Z_2}{a_0}\sqrt{\frac{\hbar^2}{2m\,E_\delta}}\right\}\right]^{-1}, \quad (51)$$

where the final wave function is normalized per unit energy range.

From these equations one obtains the differential cross section for the n^{th} shell, which per atom is

$$\frac{d\sigma_n}{dE_\delta} = \frac{2^{18}\,\pi}{5} \cdot Z_1^2 \cdot e^4 \left(\frac{m\,E_1}{M_1}\right)^4 \cdot \frac{(n\,E_B')^3}{(E_B + E_\delta)^{10}}, \quad (52)$$

where E_B' is the unscreened binding energy defined by

$$E_B' = \frac{e^2}{2\,a_0}\left(\frac{Z_2}{n}\right)^2. \quad (53)$$

In equation (52) we have omitted the last factor in (51) as it is of no practical importance. The equation is the same in the laboratory coordinates,* since $(2\,E_1 : M_1)^{1/2}$ is the velocity of the bombarding particle relative to the nucleus which is initially at rest, and since, furthermore, the center-of-mass velocity can be

* Note, however, that small center-of-mass corrections are neglected in equation (45).

neglected as compared to the velocities of the ejected electrons. Their angular distribution should, therefore, also be approximately isotropic in the laboratory system.

From the above equations, we find, as a total for all the shells, the differential cross section

$$\frac{d\sigma}{dE_\delta} = 1.0 \cdot 10^{-17} \cdot Z_1{}^2 \cdot \left(\frac{E_1}{A_1}\right)^4 \cdot Z_2{}^4 \cdot \frac{(e^2 \cdot mc^2)^2}{E_\delta{}^9} \cdot S, \tag{54}$$

where, for convenience, the rest energy mc^2 of the electron has been introduced. The sum S is given by

$$S = \sum_n \frac{1}{n^3} \cdot \frac{u^9}{(c_n + u)^{10}}, \tag{55}$$

where

$$u = \frac{E_\delta}{E_{K'}} \text{ and } c_n = \frac{E_B}{E_{K'}}. \tag{56}$$

Taking as appropriate values the figures $c_1 = 0.8$; $c_2 = 0.16$; $c_3 = 0.04$, and $c_4 = 0 = c_5 = \ldots$, we obtain the contributions shown in Fig. 15 for the various shells. They add up to a total

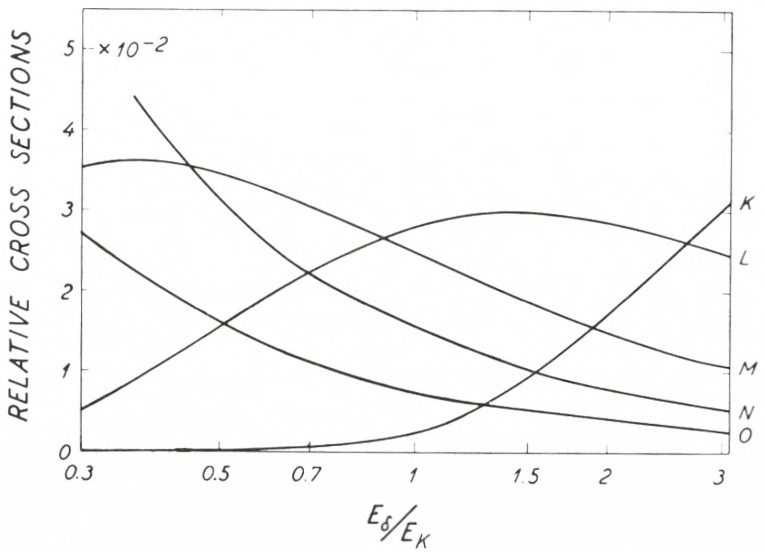

Fig. 15. Relative contributions to the stopping electrons of energy $E\delta$ from the various shells, as calculated on the basis of a non-relativistic theory neglecting screening effects.

which is nearly independent of u and has a value around 0.1 which, inserted in (54), gives the equation (35) used in Chapter III.

The comparatively good agreement between the cross sections computed from this formula and the measured ones must be somewhat coincidental. The relativistic effects appear to increase the contributions, in particular from the K shell, by large factors,§ which however will be counteracted to some extent by the effects of the screening, especially in the case of the higher shells. A correct theory would also have to take into account the higher terms in the $1/q$ expansion which, on the other hand, means that also the contributions from the p sub-shells etc. should be considered. The present derivation seems, however, to be sufficient to show the general dependence of the cross section on the various parameters and brings out the main problems necessarily involved in a more complete treatment.

Appendix II.

When free electrons are generated with an energy E_δ^* in an infinitisimal layer dx at the depth x below the surface of a target, then the fraction $W dE_\delta$ which reaches the surface by diffusion-like processes and emerges with energies between E_δ and $E_\delta + dE_\delta$, will be given by (cf. Be 2)

$$W\{E_\delta, E_\delta^*, x\}\, dE_\delta = \frac{x}{(4\pi\tau)^{1/2}} \cdot e^{-x^2/4\tau} \cdot \frac{1}{\tau} \left| \frac{d\tau}{dE_\delta} \right| dE_\delta, \qquad (57)$$

where

$$\tau\{E_\delta, E_\delta^*\} = \frac{1}{6} \int_{E_\delta}^{E_\delta^*} \lambda\{E_\delta'\} \frac{dE_\delta'}{|dE_\delta'/dx|}. \qquad (58)$$

The function τ has been tabulated by BETHE (cf. Table II of ref. Be 2), but the values given must be changed somewhat for the low electron energies which we consider here.

Firstly, the transport mean free path λ should not be calculated on the basis of the Born approximation, but rather by employ-

§ Private communication from Č. ZUPANČIČ.

ment of the classical approximation (cf., e. g., Bo 6), since for $E_\delta \approx 50$ keV and $Z_2 \approx 70$ one has the collision index

$$\varkappa^2 = 2\frac{(Z_2 \cdot e)^2}{E_\delta \cdot a_0} \approx 5 > 1. \tag{59}$$

This means that the screening cut-off takes place at a scattering angle which is $\varkappa$ times larger than in the case of the Born approximation, so that one obtains a larger λ given by

$$\left.\begin{aligned} \varrho\lambda &= 4\frac{M_0}{\pi e^4}\frac{A_2}{Z_2^2}\cdot E_\delta{}^2 \cdot \left[\log_e\left\{\frac{8\,E_\delta\,a_0}{Z_2{}^{2/3}\cdot e^2}\right\} - \log_e\left\{\varkappa^2\right\}\right]^{-1} \\ &\simeq \frac{E_\delta{}^2}{170\sqrt{Z_2}}\ \mathrm{mg/cm^2}\ \text{for}\ E_\delta\ \text{in keV}. \end{aligned}\right\} \tag{60}$$

Secondly, the specific stopping power dE_δ/dx for the electrons will, in the region which we are considering here, not be independent of the electron energy. The most probable energy loss for electrons which have travelled the distance dx will be better represented by the expression (cf., e. g., Segrè (Se 1))

$$\left.\begin{aligned} -\frac{1}{\varrho}\frac{dE_\delta}{dx} &= \frac{\pi e^4}{M_0}\cdot\frac{Z_2}{A_2}\cdot\frac{1}{E_\delta}\cdot\log_e\left\{5.5\,\frac{Z_2}{A_2}\frac{\pi a_0{}^2}{M_0}\varrho\,dx\right\} \\ &\simeq \frac{650}{E_\delta\cdot\sqrt{Z_2}}\ \frac{\mathrm{kev}}{\mathrm{mg/cm^2}}\ \text{for}\ E_\delta\ \text{in keV}, \end{aligned}\right\} \tag{61}$$

and for $\varrho\,dx \approx 0.3$ mg/cm^2.

Consequently, one obtains from equation (58) the following approximate expression for τ:

$$\varrho^2\,\tau\left\{E_\delta, E_\delta{}^*\right\} \simeq \left(\frac{E_\delta}{40}\right)^4 \cdot \left[\left(\frac{E_\delta{}^*}{E_\delta}\right)^4 - 1\right] (\mathrm{mg/cm^2})^2 \text{ for } E_\delta \text{ in keV}. \tag{62}$$

This energy dependence together with that of equation (35) for the production cross section leads, in combination with the distribution (57), to the following estimate for the yield of electrons from a target which has a thickness t/ϱ in the direction perpendicular to the surface:

$$\left.\begin{aligned} Y\{E_\delta\}\,dE_\delta &= \frac{\varrho\,dE_\delta}{A_2 M_0 \cos\theta}\int_0^{t/\varrho}\int_{E_\delta}^{\infty} W\{E_\delta, E_\delta^*, x\}\,\frac{d\sigma}{dE_\delta^*}\,dE_\delta^*\,dx \\ &= Y_\infty\,dE_\delta\,\frac{t}{t_\infty}\,\frac{1}{\sqrt{4\pi}}\int_0^{\infty}\frac{\left[1-e^{-z}\right]\cdot z^{3/2}}{\left[\left(\frac{3\sqrt{\pi}}{16}\,\frac{t}{t_\infty}\right)^2+z\right]^3}\,dz, \end{aligned}\right\} \quad (63)$$

where the effective thickness for a thick target is denoted by t_∞ and is given approximately by

$$t_\infty \simeq \frac{4}{3\sqrt{\pi}}\left(\frac{E_\delta}{40}\right)^2 \simeq \left(\frac{E_\delta}{50}\right)^2 \text{ mg/cm}^2 \quad (64)$$

if one inserts the electron energy E_δ in keV.

The dependence of the function (63) on the ratio t/t_∞ deviates less than 5 per cent from the simple exponential expression (37). In the above derivation, it has been assumed that the target support gives a back-scattering equal to that of the target material, but without contributing to the production of free electrons. Hence, the way in which the yield will actually depend on the target thickness may be somewhat different from that given by (63), even though the fact that the yield is decreasing so strongly with the energy implies a rather small back-scattering effect. Also the application of the diffusion approximation is not quite justified, and we have therefore only employed the more simple expression for comparison with the experiments.

Table I.

The figures given in the seven columns of this table have the following meaning.

1. Electron energies for the measured conversion lines. The probable errors are estimated to be about $\pm 1\ ^0/_0$.
2. Bombarding conditions; H = protons, D = deuterons, and α = He^+ ions. The bombarding energies are given in the laboratory system.
3. Target thicknesses and the materials employed by the preparation. The figures given refer only to the weight of the heavy atoms per unit area, since in many cases the amounts of light elements in the targets are not known. The values are obtained in the following ways (cf. Chapter III C).

   a) Effective layer of thick target as determined by means of Fig. 9 (angle between beam and surface equal to 45°).
   b) Thickness of target evaporated on a brass support, as determined by means of the curve $t_0 = 0$ in Fig. 7.
   c) Thickness of target prepared on a support of brass by means of the suspension method, as determined by means of the curve $t_0 = 2$ in Fig. 7.
   d) Thickness of target prepared on a support of brass by means of the suspension method, as determined by comparison with measurements on sprayed targets.
   e) Thickness of target prepared on a support of brass by means of the suspension method, as determined by weighing.

   In all other cases, the targets have been prepared either by evaporation or by means of spraying, and their thicknesses determined through measurements on the elastically scattered protons. The evaporated targets were made on a support of graphite in the case of Ta, and on copper in the case of W. The sprayed targets were made on a support of aluminum, with the exception of those used for the deuteron measurements, where brass supports were employed.
4. Total yields of conversion electrons from the 'n' shells of the atoms (n = K, L, or M). The values are computed by disregarding anisotropies, and correspond to 10^{10} projectiles. For computional reasons,

the values are given with two significant figures. The errors are estimated to be smaller than 25 per cent, except in the cases denoted with the signs $\simeq$ or $\sim$, where it may be expected that they can be as large as corresponding to factors of 1.5 and 2, respectively.

5. Assignments with respect to atomic shell and nuclear transition. Subscript 1 refers to transitions from the first collective state to the ground state; subscripts 21 and 2 refer to transitions from the second collective state to the first, and to the ground state, respectively. For composite lines, the fraction assigned to the various isotopes is given in the left-hand side of the column.
6. Transition energies for the decays corresponding to the assignments given in column 5. The binding energies have been taken from the table published by HILL *et al.* (Hi 1).
7. Partial B_{E2}-values for the various conversion lines as computed from the partial cross sections by means of equation (26). The uncertainties are indicated in the same manner as in column 4.

TABLE Ia.

$E\{n\}$	projec.	target	$Y\{n\}$	frac.	assign.		$\Delta E\downarrow$	$\varepsilon\{n\}\cdot B:e^2$
keV	A_1 MeV	mg/cm² Z_2	per 10^{10}		n	A_2	keV	10^{-48} cm⁴
118.3	H 1.75	4.3[a] Mn	$\simeq$ 5.9	1	K_1	55	124.8§	$\simeq$ 0.0009
115.2	H 1.75	4.2[a] 50 % Fe^{57}	$\sim$ 1.8	1	K_{21}	57	122.3	$\sim$ 0.0007
129.8	«	«	$\sim$ 1.2	1	K_2	57	136.9	$\sim$ 0.0004
283	H 1.75	2.7[a] Ag	$\sim$ 0.21	1	K_1	109	308	$\sim$ 0.0026
297	«	2.6[a] «	$\sim$ 0.16	1	K_1	107	322	$\sim$ 0.0023
299	«	2.6[a] Ag^{107}	$\sim$ 0.28	1	K_1	107	324	$\sim$ 0.0021
—	H 1.75	$\simeq$ 0.70[c] CeO_2	—					
—	H 1.75	$\simeq$ 0.81[c] Pr_6O_{11}	—					
88.0	H 1.75	$\simeq$ 0.51[c] Nd_2O_3	($\sim$ 0.5)	1	K_1	150	131.6	—
125.7	«	«	$\sim$ 0.36	1	L_1	150	132.4	$\sim$ 0.31
75.7	H 1.75	0.24 Sm_2O_3	16	0.8	L_1	154	83.1	2.9
«	«	«	«	0.2§	K_1	152	122.5	—
81.7	«	«	$\simeq$ 3.1	1	M_1	154	83.1	—
115.3	«	«	2.4	1	L_1	152	122.7	0.56
122.1	«	«	$\simeq$ 0.5	1	M_1	152	123.5	—
($\sim$35)	D 1.75	0.66[d] Eu_2O_3	($\lesssim$ 20)	1	K_1	153	—	—
77.0	«	«	$\simeq$ 18	1	L_1	153	84.7	—
«	H 1.75	«	9.5	1	L_1	153	«	0.65
82.9	«	«	$\simeq$ 2.4	1	M_1	153	84.3	—
$\sim$103	«	«	($\lesssim$ 0.3)	1	L_{21}	153	$\sim$ 111	($\lesssim$0.05)
146.3	«	«	$\simeq$ 0.34	1	K_2	153	194.8	$\simeq$ 0.051
$\sim$189	«	«	i	1	L_2	153	$\sim$ 196	—

§ See comments. i = indication.

TABLE Ib.

$E\{n\}$	projec.	target	$Y\{n\}$	frac.	assign.	$\Delta E\downarrow$	$\varepsilon\{n\}\cdot B:e^2$
keV	A_1 MeV	mg/cm² Z_2	per 10^{10}	n	A_2	keV	10^{-48} cm⁴
67.9	H 1.75	0.26 Gd_2O_3	15	1 L_1	160	75.7	3.4
72.7	«	«	21	0.2 M_1	160	(74)	—
«	«	«	«	0.8 L_1	158	80.5	3.4
78.9	«	«	$\simeq$ 3.9	1 M_1	158	80.4	—
83.0	«	«	11	1 L_1	156	90.8	2.8
88.4	«	«	$\simeq$ 1.9	1 M_1	156	89.9	—
116.3	«	«	$\simeq$ 0.24	1 L_1	154	124.1	$\simeq$ 0.73
49.4	D 1.75	0.58 Tb_4O_7	$\simeq$ 40	1 L_1	159	57.9	$\simeq$ 0.45
57.0	«	«	—	1 M_1	159	58.6	—
65.4	«	«	($\sim$ 10)	1 Dy	ctm	—	—
72.4	«	«	($\sim$ 13)	$\sim$ 0.5§ L_{21}	159	80.9	($\sim$ 0.2)
«	«	«	«	$\sim$ 0.5 Dy	ctm	—	—
80.3	«	«	—	$\sim$ 0.5§ M_{21}	159	81.9	—
«	«	«	—	$\sim$ 0.5 Dy	ctm	—	—
66.0	H 1.75	0.10 Dy_2O_3	10	1 L_1	164	74.6	4.8
73.1	«	«	8.3	0.3 M_1	164	(74.8)	—
«	«	«	«	0.7 L_1	162	81.7	3.2
80.2	«	«	$\simeq$ 1.2	1 M_1	162	81.9	—
39.5	D 1.75	0.31 Ho_2O_3	$\simeq$ 45	1 K_1	165	95.1	$\simeq$ 1.6
59.5	H 1.90	0.69[d] «	i	1 K_{21}	165	(115.1)	—
87.1	D 1.75	0.31 «	$\simeq$ 8.0	1 L_1	165	96.0	—
«	H 1.75	0.22 «	4.3	1 L_1	165	«	0.32
94.9	«	«	$\simeq$ 1.4	1 M_1	165	96.7	—
107.5	«	«	$\sim$ 0.32	1 L_{21}	165	116.4	$\sim$ 0.074
(156)	H 1.90	0.69[d] «	i	1 K_2	165	(212)	—

§ See comments. i = indication. ctm = contamination.

TABLE Ic.

$E\{n\}$	projec.	target		$Y\{n\}$	frac.	assign.		$\Delta E\downarrow$	$\varepsilon\{n\}\cdot B:e^2$
keV	A_1 MeV	mg/cm²	Z_2	per 10^{10}		n	A_2	keV	10^{-48} cm⁴
71.9	H 1.75	0.33	Er_2O_3	58	1	L_1	164, 166	80.8	3.6
79.3	«	«		≃ 17	1	M_1	168, 170	81.1	—
51.0	H 1.75	0.29	Tm_2O_3	≃ 28	1	K_{21}	169	110.4	≃ 2.1
101.6	«	«		4.2	1	L_{21}	169	111.2	0.32
109.7	«	«		2.4	*0.4	M_{21}	169	111.6	—
«	«	«		«	0.6	L_2	169	119.3	0.11
117.8	«	«		(~ 0.3)	1	M_2	169	119.7	—
68.3	H 1.75	0.18	Yb_2O_3	28	1	L_1	170, 172	77.9	3.9
75.0	«	«		≃ 10	1	M_1	174, 176	77.0	—
51.0	H 1.75	0.21	Lu_2O_3	≃ 17	1	K_1	175	114.3	—
104.3	«	«		≃ 3.1	1	L_1	175	114.9	0.36
112.2	«	«		~ 0.77	1	M_1	175	114.2	—
~ 80	α 1.75	≃ 1.2[e]	HfO_2†	i	1	L_1	176	90	—
84.4	H 1.75	«		≃ 110	1	L_1	178, 180	94.7	≃ 3.4†
~ 89	α 1.75	«		i	1	M_1	176	91	—
92.9	H 1.75	«		≃ 35	1	M_1	178, 180	95.0	—
104.0	«	«		≃ 4.7	1	L_1	177	114.3	≃ 0.57†
112.1	«	«		≃ 2.6	*0.4	M_1	177	114.2	—
«	«	«		«	0.6	L_1	179	122.7	0.28†
~122	«	«		i	1	M_1	179	124	—

* Cf. Fig. 2. i = indication. † Cf. footnote p. 45.

TABLE Id.

$E\{n\}$	projec.	target		$Y\{n\}$	frac.	assign.		$\Delta E\downarrow$	$\varepsilon\{n\}\cdot B:e^2$
keV	A_1 MeV	mg/cm²	Z_2	per 10^{10}	n		A_2	keV	10^{-48} cm⁴
68.7	H 2.00	0.28	Ta	17	1	K_1	181	136.2	1.4
97.4	«	«		$\simeq 0.58$	1	K_{21}	181	164.9	$\simeq 0.22$
124.4	«	«		2.6	1	L_1	181	135.9	0.21
133.5	«	«		$\simeq 0.83$	1	M_1	181	135.7	$\simeq 0.066$
153.5	«	«		~ 0.074	1	L_{21}	181	165.0	~ 0.029
34.9	α 1.45	0.35[a]	W	($\lesssim 2$)	1	L_1	183	(46.4)	—
44.3	«	«		~ 0.91	1	M_1	183	46.6	~ 0.53
89.6	H 1.75	0.23	«	7.0	0.8	L_1	182	100.4	2.7
«	«	«		«	~ 0.2	L_2	183	(~ 100)	—
100.3	«	«		6.1	0.3	M_1	182	(102.6)	—
«	«	«		«	0.6	L_1	184	111.1	1.7
111.5	«	«		3.8	0.3	M_1	184	(113.8)	—
«	«	«		«	0.7	L_1	186	122.3	1.4
121.8	«	«		$\simeq 0.55$	1	M_1	186	124.1	—
63.1	H 1.75	0.30	Re	~ 5.1	1	K_1	187	134.8	—
113.6	«	«		$\simeq 1.1$	1	L_1	185	125.7	$\simeq 0.30$
122.8	«	«		$\simeq 1.2$	0.2	M_1	185	125.2	—
«	«	«		«	0.8	L_1	187	134.9	$\simeq 0.18$
132.8	«	«		~ 0.24	1	M_1	187	135.2	—
—	H 1.75	~ 1[c]	Os	—					
116.4	H 1.75	5.0[a]	Ir	$\simeq 6.3$	1	L_1	191	129.6	$\simeq 0.12$
126.2	«	«		$\simeq 5.6$	0.2	M_1	191	128.6	—
«	«	4.8[a]	«	«	0.8	L_1	193	139.4	$\simeq 0.061$
135.4	«	«		~ 1.8	1	M_1	193	138.0	—
131.7	H 1.75	3.5[a]	Pt	~ 1.7	1	K_1	195	210.1	~ 0.15
196.4	«	«		~ 0.44	1	L_1	195	209.8	—
200.0	H 2.00	3.8[a]	Au	~ 1.9	1	K_1	197	280.7	~ 0.072
—	α 1.75	~ 0.5[b]	U	—§					

§ See comments.

Table II.

The eleven columns of this table contain:

1. Nuclei investigated.
2. Excitation energy of collective states found by the measurements.
3. Conversion lines used for the computations (cf. column 5 of Table I).
4. $K:L$ ratios obtained either from the data in Table I, or from Fig. 2, or from the results of measurements on radioactive elements (cf. Ho 1).
5. Reciprocal of the square of the mixing ratios as computed from the equation (20) and the values in column 4, or as known from other sources. (See comments).
6. Branching fractions as computed from the equation (21) and the values in column 5, or as determined directly (cf., e. g., the case $_{26}Fe^{57}$).
7. Reciprocal of the decay fractions corresponding to the modes of decay given in column 3. (Cf. Eq. (19)).
8. Total B_{E2}-values as computed from the values of column 7 and the partial B_{E2}-values of Table I. The uncertainties are indicated in the same manner as in column 4 of Table I.
9. Spin of the ground state. (Cf. Ho 1).
10. Intrinsic quadrupole moments as computed from equations (7) and (8).
11. Gyromagnetic ratios computed by means of equation (15). (Note the discussion in Chapt. V).

Where the mixing ratios are only known to lie within certain limits, the values given in columns 7, 8, and 10 are those corresponding to the two limits, with the $M1$ limit given first.

TABLE IIa.

nucleus	level keV	line n	$K:L$	$1:\delta^2$	β	$1:\varepsilon\langle n\rangle$	$B:e^2$ 10^{-48} cm^4	I_0	Q_0 10^{-24} cm^2	$\lvert g_K-g_R\rvert$
$_{25}Mn^{55}$	125§	K_1	$\gtrsim 7$	—	1	64 6.6	$\simeq 0.057$ $\simeq 0.006$	3/2	1.1 (0.4)†	—
$_{26}Fe^{57}$	137	K_{21}	—	$\gtrsim 10$§	0.92§	65	~ 0.044	1/2	0.9	—
«	137	K_2	—	0	0.08§	100				
$_{47}Ag^{107}$	323	K_1	—	—	1	78 53	~ 0.17 ~ 0.12	1/2	2.1 1.7	—
$_{47}Ag^{109}$	308	K_1	—	—	1	67 50	~ 0.18 ~ 0.13	1/2	2.1 1.8	—
$_{60}Nd^{150}$	132	L_1	*1.4	0	1	5.1	~ 1.6	0	4.0	
$_{62}Sm^{152}$	123	L_1	*1.1	0	1	4.0	2.3	0	4.8	
$_{62}Sm^{154}$	83	L_1	*0.57	0	1	2.2	6.2	0	7.9	
$_{63}Eu^{153}$	84	L_1	~ 1	~ 0.4	1	2.5	1.6	5/2	5.8	$\lesssim 0.1$
«	195	L_{21}	—	«	(~ 0.35)	(~ 11)	($\lesssim 0.6$)	5/2	—	
«	195	K_2	*2.2	0	$\simeq 0.65$	11	$\simeq 0.56$	5/2	5.8§	
$_{64}Gd^{154}$	124	L_1	*1.0	0	1	3.8	$\simeq 2.8$	0	5.3	
$_{64}Gd^{156}$	90	L_1	*0.59	0	1	2.3	6.0	0	7.8	
$_{64}Gd^{158}$	80	L_1	*0.48	0	1	2.0	6.5	0	8.1	
$_{64}Gd^{160}$	76	L_1	*0.43	0	1	1.9	6.4	0	8.1	
$_{65}Tb^{159}$	58	L_1	—	($\gtrsim 50$)§	1	7.7§	$\simeq 3.5$	3/2	8.3	
«	139	L_{21}	—	«	$\gtrsim 0.95$§	—	—	3/2	—	$\gtrsim 2$
$_{66}Dy^{162}$	82	L_1	*0.43	0	1	1.9	6.1	0	7.9	
$_{66}Dy^{164}$	75	L_1	*0.37	0	1	1.8	8.5	0	9.2	
$_{67}Ho^{165}$	96	L_1	$\simeq 4.9$	~ 11	1	$\simeq 7.7$	$\simeq 2.5$	7/2	7.7	0.51
«	212	L_{21}	—	«	0.9	$\simeq 10$	~ 0.76	7/2	8.4	

§ See comments. * Cf. Fig. 2.

TABLE IIb.

nucleus	level keV	line n	$K:L$	$1:\delta^2$	β	$1:\varepsilon\{n\}$	$B:e^2$ 10^{-48} cm^4	I_0	Q_0 10^{-24} cm^2	$\lvert g_K - g_R\rvert$
$_{68}$Er even	81	L_1	*0.37	0	1	1.9	6.8	0	8.3	
$_{69}$Tm^{169}	119	K_{21}	$\simeq 6.5$	$\gtrsim 20$	0.9	1.8	3.7	1/2	7.9	—
«	119	L_2	*0.69	0	~ 0.09§	~ 34				
$_{70}$Yb even	77	L_1	*0.25	0	1	1.8	6.8	0	8.3	
$_{71}$Lu^{175}	114	L_1	$\simeq 5.5$	(~ 20)§	1	8.9	3.2	7/2	8.8	(~ 1.0)§
$_{72}$Hf^{177}	114	L_1	$\lesssim 2$	$\lesssim 0.02$§	1	(2.6)	~ 1.5§	7/2§	6.0	$\lesssim 0.03$§
$_{72}$Hf^{178}										
$_{72}$Hf^{180}	95	L_1	*0.38	0	1	2.0	$\simeq 6.9$†	0	8.3†	
$_{73}$Ta^{181}	136	K_1	6.5	7.0§	1	1.7	2.3	7/2	7.3	0.56
«	301	K_{21}	~ 7	7.1§	0.80§	2.8	$\simeq 0.62$	7/2	7.6	
$_{74}$W^{182}	100	L_1	*0.36	0	1	2.0	5.5	0	7.5	
$_{74}$W^{183}	46	M_1+N_1		—	1	5.3§	~ 2.8	1/2	8.4	—
$_{74}$W^{184}	112	L_1	*0.45	0	1	2.3	4.0	0	6.4	
$_{74}$W^{186}	123	L_1	*0.54	0	1	2.7	3.8	0	6.2	
$_{75}$Re^{185}	125	L_1	—	—	1	9.2 2.7	$\simeq 2.7$ $\simeq 0.81$	5/2	7.6 4.2	—
$_{75}$Re^{187}	135	L_1	$\simeq 5.1$	~ 8.7	1	8.7	$\simeq 1.6$	5/2	5.8	0.63
$_{77}$Ir^{191}	129	L_1	2.1§	0.86	1	4.8	$\simeq 0.56$	3/2	3.3	0.29
$_{77}$Ir^{193}	139	L_1	3.7§	3.6	1	6.2	$\simeq 0.38$	3/2	2.7	0.53
$_{78}$Pt^{195}	210	K_1	~ 3.8	~ 1	1	3.2	~ 0.47	1/2	3.4	—
$_{79}$Au^{197}	281	K_1	$\gtrsim 3$	∞ $\simeq 1.7$§	1	3.2 4.2§	~ 0.23 ~ 0.30	3/2	2.1 2.4	$\gtrsim 0.36$

§ See comments. §) Cf. Fig. 2. † Cf. footnote p. 45.

TABLE III.

Comparison of the B-values from the present Coulomb excitation measurements (summarized in Table II and repeated here in column 5) with those (column 4) computed from the half-lives (column 3) by means of equations (30) and (31). The half-lives have been taken from the tables published by SUNYAR (Su 1).

Nucleus	$h\nu$	$\tau_{1/2}$	$B_{E2}: e^2$ (from $\tau_{1/2}$)	$B_{E2}: e^2$ (from C. E.)
Z_2	keV	10^{-9} sec.	10^{-48} cm^4	10^{-48} cm^4
$_{62}Sm^{152}$	122	1.4	3.3	2.3†
$_{64}Gd^{154}$	123	1.2	3.4	$\simeq$ 2.8†
$_{66}Dy^{160}$	85	1.8	5.0	—
$_{66}Dy^{162}$	82	—	—	6.1
$_{68}Er^{164}$	90	1.4	5.5	—
$_{68}Er^{166}$	81	1.7	6.0	6.8
$_{70}Yb^{170}$	84	1.57	5.2	6.8
$_{72}Hf^{176}$	89	1.35	5.1	—
$_{72}Hf^{180}$	93	1.4	4.8	$\simeq$ 6.9
$_{74}W^{182}$	100	1.27	4.1	5.5

† The values will be relatively higher if the $K:L$ ratios are increased (cf. footnote p. 12).

References*.

Al 1 K. ALDER, A. BOHR, T. HUUS, B. R. MOTTELSON, A. WINTHER; a review article on Coulomb excitation, to be submitted to Rev. Mod. Phys.

Al 2 K. ALDER and A. WINTHER, Phys. Rev. **96**, 237 (1954); Dan. Mat. Fys. Medd. **29**, no. 19 (1955); CERN/T/KA-AW-4 (1955).

Al 3 D. E. ALBURGER and M. A. GRACE, Proc. Phys. Soc. A **67**, 280 (1954).

Be 1 H. A. BETHE, Ann. d. Phys. **5**, 325 (1930).

Be 2 H. A. BETHE, M. E. ROSE, and L. P. SMITH, Proc. Amer. Phil. Soc. **78**, 573 (1938).

Bi 1 L. C. BIEDENHARN and M. E. ROSE, Rev. Mod. Phys. **25**, 729 (1953).

Bj 1 J. H. BJERREGAARD and T. HUUS, Phys. Rev. **94**, 204 (1954).

Bo 1 A. BOHR and B. R. MOTTELSON, Dan. Mat. Fys. Medd. **27**, no. 16 (1953).

Bo 2 A. BOHR and B. R. MOTTELSON, Dan. Mat. Fys. Medd. **30**, no. 1 (1955).

* For a complete list, the reader is referred to the review article (Al 1).

Bo 3 F. Boehm, P. Marmier, and J. W. M. DuMond, Phys. Rev. **95**, 864 (1954).
Bo 4 A. Bohr and B. R. Mottelson, Chapter 17 'Beta- and Gamma-Ray Spectroscopy', ed. by K. Siegbahn, North-Holland Publ. Co. (1955).
Bo 5 A. Bohr, Dissertation (Einar Munksgaards Forlag, Copenhagen 1954).
Bo 6 N. Bohr, Dan. Mat. Fys. Medd. **18**, No. 8 (1948).
Br 1 K. J. Broström, T. Huus, and R. Tangen, Phys. Rev. **71**, 661 (1947).
Br 2 B. M. Brown and D. H. Tomboulian, Phys. Rev. **88**, 1158 (1952).

Fo 1 K. W. Ford, Phys. Rev. **95**, 1250 (1954).

Gl 1 K. M. Glover and P. Borrel, J. Nucl. Energy, 1, 215 (1955).

Gu 1 T. Gustafson, Dan. Mat. Fys. Medd. **30**, no. 5 (1955).

He 1 N. P. Heydenburg and G. M. Temmer, Phys. Rev. **100**, 150 (1955); (cf. also Phys. Rev. **93**, 906 (1954).
He 2 N. P. Heydenburg and G. M. Temmer, Phys. Rev. **95**, 861 (1954).
He 3 W. Henneberg, Z. f. Phys. **86**, 592 (1933).
Hi 1 R. D. Hill, E. L. Church, and J. W. Mihelich, Rev. Sci. Instr. **23**, 523 (1952).
Ho 1 J. M. Hollander, I. Perlman, and G. T. Seaborg, Rev. Mod. Phys. **25**, 469 (1953).
Hu 1 T. Huus and Č. Zupančič, Dan. Mat. Fys. Medd. **28**, no. 1 (1953).
Hu 2 T. Huus and A. Lundén, Phil. Mag. **45**, 966 (1954).
Hu 3 T. Huus and J. H. Bjerregaard, Phys. Rev. **92**, 1579 (1953).

Jo 1 S. A. E. Johannson, private communication.

Ka 1 T. Kamei, private communication to A. Bohr.
Ke 1 A. Kerman, Dan. Mat. Fys. Medd. 29, no. 15 (1955).
Ko 1 O. Kofoed-Hansen, J. Lindhard and O. B. Nielsen, Dan. Mat. Fys. Medd. **25**, no. 16 (1950).

Li 1 J. Lindhard and M. Scharff, Dan. Mat. Fys. Medd. **27**, no. 15 (1953).
Li 2 K. H. Lindenberger and A. Steudel, Naturwiss. **42**, 41 (1955).

Ma 1 H. Mark, private communication.
Ma 2 C. B. Madsen, Dan. Mat. Fys. Medd. **27**, no. 13 (1953).
Ma 3 N. Marty, C. R. **238**, 2516 (1954).
Ma 4 P. Marmier and F. Boehm, Phys. Rev. **97**, 103 (1955).
Mc 1 C. L. McClelland, H. Mark, and C. Goodman, Phys. Rev. **97**, 1191 (1955).

Mc 2 C. L. McClelland, private communication.
Mc 3 F. K. McGowan and P. H. Stelson, Phys. Rev. **99**, 127 (1955).
Mc 4 C. L. McClelland, H. Mark and C. Goodman, Phys. Rev. **93**, 904 (1954).
Mo 1 B. R. Mottelson and S. G. Nilsson, Phys. Rev. **99**, 1615 (1955).
Mo 2 B. R. Mottelson and S. G. Nilsson, to appear in Dan. Mat. Fys. Medd.
Mu 1 J. J. Murray, P. Snelgrove, P. E. Marmier, and J. W. M. DuMond, Phys. Rev. **96**, 858 (1954).

Ni 1 S. G. Nilsson, Dan. Mat. Fys. Medd. **29**, no. 16 (1955).

Ro 1 M. E. Rose, G. H. Goertzel, B. I. Spinrad, J. Harr, and P. Strong, Phys. Rev. **83**, 79 (1951).
Ro 2 M. E. Rose, L. C. Biedenharn, and G. B. Arfken, Phys. Rev. **85**, 5 (1952).

Sa 1 D. Saxon, Phys. Rev. **81**, 639 (1951).
Se 1 E. Segrè, Experimental Nuclear Physics I (J. Wiley and Sons, New York 1953).
Si 1 B. E. Simmons, P. M. van Patter, K. F. Famularo, and R. V. Stuart, Phys. Rev. **97**, 89 (1955).
So 1 A. Sommerfeld, Atombau und Spektrallinien II (F. Vieweg und Sohn, Braunschweig 1939).
St 1 P. H. Stelson and F. K. McGowan, Phys. Rev. **99**, 112 (1955).
Su 1 A. W. Sunyar, Phys. Rev. **98**, 653 (1955).

Te 1 G. M. Temmer and N. P. Heydenburg, private communication.

Wa 1 H. de Waard, Dissertation (Uitgeverij Excelsior, The Hague, 1954).

Zu 1 Č. Zupančič and T. Huus, Phys. Rev. **94**, 205 (1954).

Indleveret til selskabet den 15. august 1955.
Færdig fra trykkeriet den 27. februar 1956.